PROTEASE-RESISTANT ADAMTS13 MUTANTS

CHARACTERIZING PROTEASE-RESISTANT ADAMTS13 MUTANTS

By VERONICA DEYOUNG, B.H.Sc. (Hon.)

A Thesis Submitted to the School of Graduate Studies in Partial Fulfilment of the Requirements for the Degree Master of Science

McMaster University MASTER OF SCIENCE (2023) Hamilton, Ontario (Medicine)

TITLE: Characterizing Protease-Resistant ADAMTS13 Mutants

AUTHOR: Veronica DeYoung, B.H.Sc. (McMaster University)

SUPERVISOR: Dr. C. Kretz

NUMBER OF PAGES: xii, 83

LAY ABSTRACT

Current drugs used to dissolve blood clots can cause major bleeding. Therefore, safer treatments need to be developed. An important step in the clotting pathway is platelet accumulation in the injured vessel. Platelets stick to string-like protein, von Willebrand Factor (VWF), and ADAMTS13 is a protein that regulates this by cutting VWF strings. ADAMTS13 shows promise as a treatment for clots without causing bleeding, but it is unclear how its activity is controlled. ADAMTS13 can be degraded by other proteins, however the importance of this process in the body is unknown. This work characterizes a degradation-resistant ADAMTS13 mutant, which may be used to study whether ADAMTS13 degradation reduces its therapeutic effectiveness. The mutant has normal VWF-cutting activity, is resistant to degradation by clotting proteins, and is partially resistant to proteins released by neutrophils, an important immune cell in clotting. Future studies will investigate its effectiveness at treating clots in animals.

ABSTRACT

ADAMTS13 is a metalloprotease that regulates the length, and thus, the platelet-capturing capacity of von Willebrand factor. The regulation of ADAMTS13 activity remains poorly understood. Numerous circulating proteases cleave ADAMTS13 *in vitro,* impairing its activity, but the physiological significance of this mechanism remains unknown. Two commonly cleaved regions within ADAMTS13 were identified and mutants were developed: two with one of each region mutated (T4L and T8L mutants), one with both regions mutated (T4L/T8L or "double" mutant), and one with an additional elastase site mutated (T4L/T8L + I380G). This work characterizes the mutants' resistance to proteolysis and compares the activity of the double mutant to wild-type ADAMTS13 (WT).

Each mutant and WT was incubated with purified coagulation and neutrophil proteases, activated neutrophils, or added to plasma before initiating coagulation with or without tissue plasminogen activator. Cleavage patterns were visualized with western blot. FRETS-VWF73 and microfluidic flow assays were used to compare WT and mutant activity.

Coagulation proteases cleave both predicted sites within WT, and the double mutant exhibits near complete resistance to cleavage over 3 hours. Resistance to degradation by neutrophil proteases is prolonged in the double mutant, but additional cleavage sites are present. Elastase cleavage is prevented in the T4L/T8L + I380G mutant. In plasma, WT is degraded upon initiating coagulation and subsequent

fibrinolysis, which is prevented in the double mutant. WT is also degraded in the presence of activated neutrophils, and the double and T4L/T8L + I380G mutants exhibit improved but incomplete resistance. Finally, the mutants exhibit similar activity to WT using FRETS-VWF73 and the microfluidic assay.

This work validates the location of two protease-sensitive regions within ADAMTS13 and confirms the resistance of the double mutant to coagulation proteases *in vitro*. Future work will complete the activity analysis, and compare the mutants' therapeutic efficacy to WT *in vivo*.

ACKNOWLEDGMENTS

Pursuing my Master's in the Thrombosis and Atherosclerosis Research Institute (TaARI) at McMaster University was an unforgettable experience that has helped me to grow significantly, both personally and professionally. I would first like to thank my supervisor, Dr. Colin Kretz, for his incredible mentorship. Allowing me to experiment and problem-solve independently, while providing guidance to keep me on the right track, has fostered my love for research. It has also helped me to build foundational critical thinking skills which I strive to continue improving through my future endeavors.

I am extremely grateful for the support provided by my lab members, Cherie Teney, soon-to-be Dr. Taylor Sparring, Dr. Hasam Madarati, Dr. Kanwal Singh, and Peter Andrisani, who helped me navigate the unfamiliar wet lab setting and overcome hurdles as they came. Given the collaborative atmosphere at TaARI, support came from all angles – thank you to all members of the adjacent labs, especially Rida Malik, Paul Tieu, Erblin Cani, Neha Sharma, and Jim Fredenburgh, for answering my many questions and sharing your expertise. Thank you to my committee members as well, Dr. Peter Gross and Dr. Davide Matino, for helping me to identify the gaps in my work.

Finally, to the incredible friends I have met that have made my time at TaARI such a memorable and happy experience – all those previously mentioned, as well as Sean Carlin, Dr. Sarah Medeiros, Mikaela Eng, Graham Rix, Bhavishya Challagundla, Keshikaa Suthaaharan – thank you for always keeping the morale high throughout the past two years. I look forward to seeing you achieve your goals!

TABLE OF CONTENTS

LISTS OF FIGURES AND TABLES

LIST OF ABBREVIATIONS

ACD	acid citrate dextrose solution
ADAMTS13	a disintegrin and metalloproteinase with a thrombospondin type-1 motif, member 13
C	cysteine-rich domain
caADAMTS13	constitutively active ADAMTS13 mutant
CHO	Chinese hamster ovary cells
crADAMTS13	commercial recombinant ADAMTS13
D	disintegrin-like domain
DIC	disseminated intravascular coagulation
DMEM	Dulbecco's Modified Eagle Medium
DPBS	Dulbecco’s Phosphate-Buffered Saline buffer
ELISA	enzyme-linked immunosorbent assay
F	factor
FBS	fetal bovine serum
FRETS-VWF73	fluorescence resonance energy transfer substrate von Willebrand Factor 73
GoF-ADAMTS13	gain-of-function ADAMTS13 mutant
HEK	human embryonic kidney
HK	high molecular weight kininogen
HRP	horseradish peroxidase
HUVEC	human umbilical vein endothelial cells
M	metalloprotease domain
MCAo	middle cerebral artery occlusion
MWCO	molecular weight cut-off
NET	neutrophil extracellular trap
PBS	phosphate-buffered saline
PCPS	phosphatidylcholine-phosphatidylserine lipid vesicles
PGI2	prostaglandin I2
PMA	phorbol myristate acetate
PRP	platelet-rich plasma
RPMI	Roswell Park Memorial Institute
S	spacer domain
SDS-PAGE	sodium dodecyl-sulfate polyacrylamide gel electrophoresis
T or TSP1	thrombospondin type-1 repeat

T2L	linker region following second thrombospondin type-1 repeat of ADAMTS13
T4L	linker region following fourth thrombospondin type-1 repeat of ADAMTS13
T8L	linker region following eighth thrombospondin type-1 repeat of ADAMTS13
TBS	Tris-buffered saline
TBST	Tris-buffered saline with Tween20
TF	tissue factor
tPA	tissue plasminogen activator
TTP	thrombotic thrombocytopenic purpura
UL	ultra-large
uPAR	urokinase-type plasminogen activator receptor
VWD	von Willebrand's Disease
VWF	von Willebrand Factor
VWF115	synthetic 115-amino acid peptide derived from von Willebrand Factor
WT	wild-type

1. INTRODUCTION

1.1 Overview of hemostasis

Hemostasis is the physiological process leading to blood clot formation at sites of vascular injury. Blood vessels are lined with endothelial cells that help to maintain blood fluidity under normal conditions[1]. Disruption of the endothelial layer, intrinsically or extrinsically, generates procoagulant components that activate a tightly regulated hemostatic pathway. This can result from physical vascular damage, components of the innate and adaptive immune system pathways, and health conditions affecting the components of the coagulation system (e.g., coagulation factor deficiencies, atherosclerosis)[2]. Disruption of the balance between these pathways can lead to excessive bleeding or thrombosis, both of which can cause inadequate blood supply to tissues and subsequent cell death. The three major components of the hemostatic process are referred to as primary hemostasis, secondary hemostasis, and fibrinolysis, or tertiary hemostasis[3].

Primary hemostasis refers to the recruitment of platelets to the site of vessel injury to form the primary platelet plug. Upon injury, procoagulant subendothelial components are exposed to the vessel lumen. This includes collagen, which can bind and tether circulating multimeric glycoprotein von Willebrand factor (VWF) to the vessel wall. Circulating platelets can then bind VWF and subsequently bind collagen to adhere more firmly under conditions of high shear (e.g., arterioles), or can bind collagen directly in lower flow rates (e.g., veins)[4-6]. Upon binding, platelets activate and release agonists in a

positive feedback mechanism that further recruits platelets to the area[7]. Platelets continue to build up at the site of injury, forming a "plug" that stops blood from leaving the vessel. This plug requires further stabilization through the deposition of insoluble fibrin to form a clot, which occurs simultaneously. Fibrin is generated by the coagulation cascade, a process referred to as secondary hemostasis (Figure 1)[3].

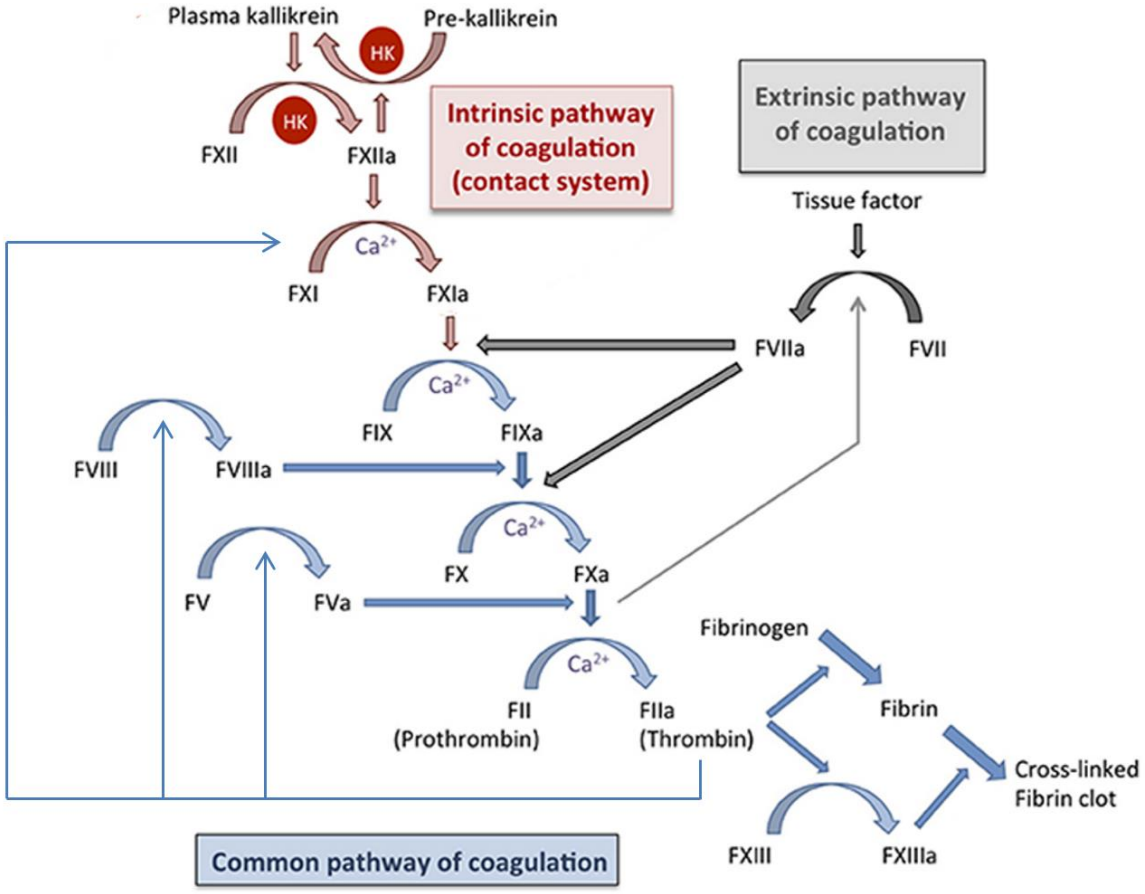

Figure 1. Overview of secondary hemostasis. The common pathway of coagulation (blue arrows) is activated via the intrinsic pathway (red arrows) or the extrinsic pathway (gray arrows). The common pathway generates factor Xa, which converts prothrombin to thrombin in the presence of its cofactors. Thrombin then converts fibrinogen into fibrin and generates factor XIIIa, which cross-links and stabilizes the fibrin clot. Thin arrows indicate catalysis of upstream

reactions. Coagulation factors are indicated with "F" followed by a roman numeral, and "a" denotes the activated form; HK, high molecular weight kininogen. Figure adapted from Loof, Deicke, & Medina[8].

Secondary hemostasis refers to stepwise activation of coagulation serine proteases that culminates in the cleavage of soluble fibrinogen into insoluble fibrin by thrombin. Fibrinogen is incorporated into and around the platelet plug, forming a clot-stabilizing mesh when converted to fibrin and crosslinked by activated factor XIII (factor XIIIa)[9]. This mechanism is activated via two separate pathways that converge at the generation of factor Xa: the intrinsic and extrinsic pathways. The intrinsic pathway, coined due to its activation within the lumen without requiring contact with extravascular components, is initiated by the activation of factor XII. This can occur in the presence of negatively charged molecules or surfaces, such as phosphatidylserine expressed on activated platelets[10]. Factor XIIa can activate circulating prekallikrein to form kallikrein, a more potent factor XII activator in the presence of circulating high molecular weight kininogen[11]. Factor XIIa then generates factor XIa, which generates factor IXa, which finally activates factor X in the presence of its cofactor, factor VIIIa.

The extrinsic pathway is initiated when the vessel wall is damaged, exposing the lumen to extravascular tissues rich in tissue factor. Tissue factor forms a complex with factor VIIa, which activates factor X. Factor Xa, generated by both pathways, forms a complex with its cofactor, factor Va, to cleave prothrombin, forming thrombin (factor IIa)[3]. Thrombin can generate fibrin, amplify upstream steps in the coagulation cascade, and contribute to platelet activation[12]. Under normal physiological conditions, this leads

to the formation of a stable clot at the site of injury that stops bleeding and allows for vessel repair.

Tertiary hemostasis is the process responsible for clearing the blood clot during wound repair and preventing vessel occlusion. This is achieved by fibrinolysis, or the breakdown of fibrin, which is catalyzed by plasmin. Plasmin is generated when circulating plasminogen is cleaved by one of two enzymes: tissue-type plasminogen activator (on the surface of a fibrin clot) or urokinase-type plasminogen activator (in the presence of its cell-surface receptor, urokinase-type plasminogen activator receptor [uPAR])[13].

1.2 von Willebrand factor

An important component of primary hemostasis is VWF (Figure 2). VWF is a large (~270 kDa) multimeric, multidomain glycoprotein[14] that acts as both a carrier for coagulation factor VIII, and as an adhesive link between platelets and the injured vessel wall[15 16]. Upon vascular injury, VWF can bind to exposed subendothelial collagen type I or III via its A3 domain, or collagen type IV via its A1 domain[17]. This binding increases its affinity for the GPIbα chain within the GPIb-V-IX receptor complex on the surface of circulating platelets[18] in the presence of sufficient shear stress imposed by blood flow as follows. VWF unravels from a globular form with low binding affinity for platelets, to an elongated, “string-like” form, with exposed platelet-binding A1 domains[19-21]. Platelets can bind to tethered VWF strings, bringing them within closer proximity to collagen.

Upon binding collagen, platelets activate, releasing various agonists that help to recruit and activate additional platelets in a positive feedback mechanism. This forms the primary platelet plug.

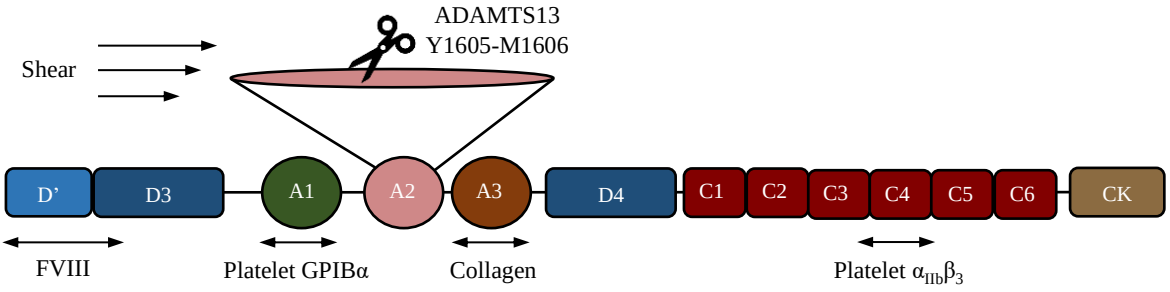

Figure 2. VWF monomer domain organization and interaction sites. Arrows refer to the binding site of the indicated structure. Scissors refer to the scissile bond within the A2 domain of VWF at which ADAMTS13 cleaves in the presence of sufficient shear stress.

VWF is synthesized in megakaryocytes[22] and endothelial cells[23] as monomers that dimerize via disulfide bridges connecting C-terminal CK domains, and multimerize via disulfide bridges connecting D3 domains, closer to the N-terminus. This connects monomers in a "head-to-head" and "tail-to-tail" fashion[24]. In endothelial cells, VWF is constitutively secreted and cleaved to varying lengths by its primary molecular regulator, ADAMTS13, creating a "hemostatically balanced" distribution of multimer lengths under normal conditions. VWF is also stored in endothelial cell Weibel-Palade bodies as predominantly ultra-large multimers, which can exceed 20,000 kDa[14 25]. When endothelial cells become activated in response to various agonists generated upon vascular injury, Weibel-Palade body contents are released into the vessel lumen[26 27]. VWF synthesized in megakaryocytes is primarily stored in platelet α-granules as mostly

UL and large multimers, which are released upon platelet activation[6 28]. Normal physiological VWF multimer length distribution and their hemostatic potential are outlined in Figure 3.

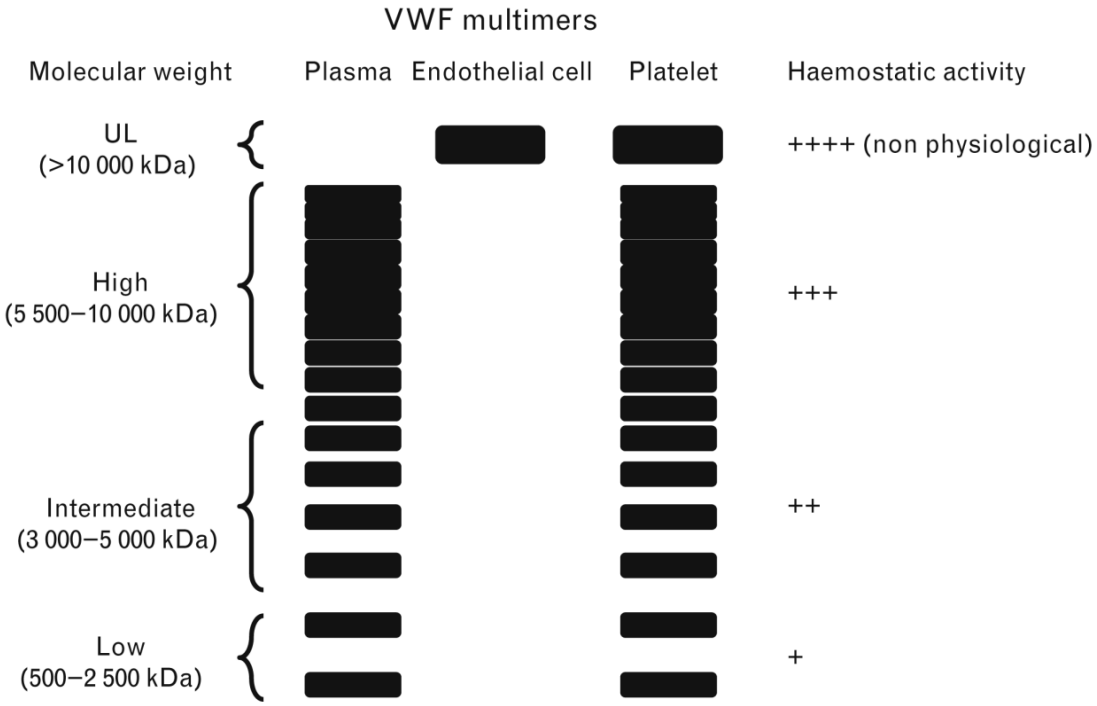

Figure 3. Physiological VWF multimer distribution and hemostatic activity. Plasma-derived VWF is constitutively secreted from endothelial cells and cleaved to varying lengths by ADAMTS13. Endothelial cell-derived VWF is stored as ultra-large multimers in Weibel-Palade bodies, which are released into the lumen upon endothelial activation. Platelet-derived VWF is stored in α-granules primarily as UL and high molecular weight VWF multimers, which are released upon platelet activation and degranulation. VWF activity, in terms of collagen- and platelet-binding affinity, is dependent on multimer length, as indicated in the figure (low to high = + to ++++). UL, ultra-large. Figure obtained from Stockschlaedera, Schneppenheimb & Budde[29].

The magnitude of VWF-mediated hemostatic potential increases with the length of VWF multimers and the level of shear stress applied. Longer VWF multimers possess

more platelet- and self-binding domains and increase drag at the endothelial surface, allowing for more contact with circulating platelets[15 30]. Shear stress unravels VWF multimers to allow for platelet adhesion and self-association[31 32]. Due to smaller vessel size and high shear force imposed by blood flow, the highest levels of shear stress are found at the vessel wall of arterioles, followed by arteries, venules, then veins[33]. Due to this effect of vessel size, stenosis can constitute higher shear stress, and thus prothrombotic conditions[34]. VWF length, and thus its thrombotic potential, is regulated by the circulating metalloprotease, ADAMTS13 (a disintegrin and metalloprotease with thrombospondin type 1 repeats, member 13)[35]. Cleavage of VWF by ADAMTS13 occurs in its A2 domain at the Y1605-M1606 bond[36]. which is only accessible upon shear-induced unravelling of VWF[37].

1.3 Shear-dependent regulation of von Willebrand factor by ADAMTS13

Circulating VWF multimers exist primarily in a globular form. Under conditions of shear stress ranging from approximately 35 – 70 dyn/cm^2, the attractive forces between monomers are overcome by drag and VWF transiently unravels and recompresses, which may allow for ADAMTS13 cleavage in circulation[38]. This transient unravelling occurs more frequently as VWF multimers become larger, a mechanism that further ensures ultra-large, hemostatically active VWF multimers are cleared more quickly from circulation. However, VWF cleavage by ADAMTS13 is more likely to occur at the vessel wall, where VWF is tethered and shear stress is highest. Thus, ADAMTS13 cleaves VWF during secretion from endothelial cells to establish a hemostatically balanced distribution

of multimer lengths[39 40], and at sites of vascular injury where VWF-platelet strings are adhered[33].

The cleavage site for ADAMTS13 within the VWF A2 domain is cryptic under static conditions, and is exposed when shear stresses exceed 10 pN of force across the domain[38 40]. A vicinal cysteine pair, C1669/C1670, forms a disulfide bond that helps to stabilize the A2 domain, providing a narrow window of shear conditions conducive to unfolding[33 41]. This structural stabilization further limits the opportunity for ADAMTS13 to cleave VWF. Once unraveled, multiple exosite interactions between ADAMTS13 and the VWF A2 domain stabilize its denatured conformation and align the scissile bond within the active site[42].

1.4 ADAMTS13

1.4.1 Structural characteristics of ADAMTS13

ADAMTS13 is a metalloprotease in the Metzincin protease superfamily[43] predominantly synthesized in hepatic stellate cells[44] in addition to glomerular endothelial cells, lung cells, and spleen cells to a lesser degree[44 45]. ADAMTS13 has a molecular weight of ~180-200 kDa[46] and a normal physiological blood concentration of approximately 1 μg/mL or 5 nM[47]. ADAMTS13 possesses multiple domains: the metalloprotease (M) domain, the disintegrin-like (D) domain, the first thrombospondin type-1 repeat (TSP1) domain, the cysteine-rich (C) domain, and the spacer (S) domain, followed by a TSP-1 domain, a T2-linker region (T2L), 2 TSP-1 domains, a T4-linker

(T4L) region, 4 more TSP1 domains, a T8-linker (T8L) region, and 2 C-terminal CUB domains (CUB-1 and CUB-2)[48] (Figure 4).

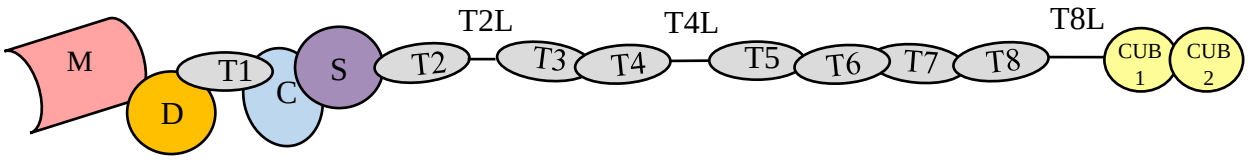

Figure 4. ADAMTS13 domain organization from N to C terminals. M = metalloprotease domain, D = disintegrin-like domain, T = thrombospondin type 1-repeats (also referred to as TSP1-1 through -8), C = cysteine-rich domain, S = spacer domain, CUB1 and CUB2 = CUB domains. T2L, T4L, and T8L indicate linker regions. Constructed based on structural predictions published by Zheng[48].

Prior to secretion, the signal peptide and propeptide preceding the M domain are removed[49]. In contrast to most other ADAMTS proteases, the propeptide is short and its removal is not required to achieve normal proteolytic activity[48 49]. Mutagenesis studies of ADAMTS13 lacking the propeptide demonstrated normal synthesis and secretion[49], thus whether it serves a function or is merely a remnant of evolution remains unclear. Moreover, ADAMSTS13 is a heavily glycosylated protein, containing N-, O- and C-linked glycans that contribute to 20% of its mass[50-52]. N-linked glycosylation and O-linked fucosylation are imperative to proper folding and secretion of ADAMTS13[52 53]. Numerous N-linked glycans also help to facilitate the closed conformation (outlined in section 1.4.3) and protect against binding of autoantibodies. While the effects of O- and C-linked glycosylation on ADAMTS13 activity remain unclear, they may be important in immune recognition and clearance[51 54].

1.4.2 N-terminal ADAMTS13 exosite interactions with VWF

The M domain contains the active site of ADAMTS13 that catalyzes hydrolysis of the VWF scissile bond. The active site consists of 3 histidine residues (amino acids 224, 228, and 234) that coordinate a Zn^{2+} ion, and the E225 residue, which forms a hydrogen bond with the water molecule required for VWF hydrolysis[42]. There are also three putative Ca^{2+} binding sites, one of which has been shown to be integral to the protein's proteolytic activity[55]. VWF is the only known substrate of ADAMTS13, and its proteolysis is highly complex, depending on multiple exosite interactions[42]. The metalloprotease domain alone has little to no proteolytic activity, and activity increases as more of the non-catalytic domains are added[56-58].

The D, C, and S domains contain important exosites that align shear-activated VWF within the ADAMTS13 active site for proteolysis[56-59]. The presence of shear stress unravels the VWF A2 domain by pulling apart a disulfide bridge that connects the domain's C- and N-terminal ends, exposing exosite binding residues. Many of these binding sites have been mapped. ADAMTS13 residues R660/Y661/Y665 in the S domain bind E1660-R1668 residues within the VWF A2 domain. Subsequently, R349 in the D domain binds D1614 in the A2 domain, which helps to align the scissile bond with the M domain for subsequent cleavage[42]. The C domain has three surface loops at D454-H469, V474-A481, and M509-T518 that are shown to be important for binding VWF in an area localized to residues 1642-1654[57 58], but the precise residues and the nature of this interaction remain unclear.

Studies support the importance of these exosite interactions to VWF cleavage by performing ADAMTS13 mutagenesis and measuring the rate of VWF cleavage. Substitution of the S domain residues responsible for binding VWF reduces proteolysis of VWF115 substrate by 12.5-fold, and binding by 25-fold under static conditions[60]. These mutations also reduced proteolysis of full-length VWF under static denaturing conditions[60]. Notably, mutation of this specific exosite in the S domain of ADAMTS13 only minimally impacts proteolysis of full-length multimeric VWF under flow, suggesting that other exosite interactions may compensate for this loss under physiological conditions[60]. Mutations in the D domain, R349A and L350G, each diminish VWF115 cleavage and binding by up to 20-fold, and reduced proteolysis of full-length VWF under denaturing conditions compared to wild-type ADAMTS13[61]. Mutation of the aforementioned C domain surface loops also diminish proteolytic activity toward VWF73[58].

1.4.3 C-terminal ADAMTS13 exosite interactions with VWF

Current perspectives on the function of the C-terminal TSP1 and CUB-1/-2 domains are focused on two mechanisms; first, they play a role in the binding of VWF under physiological conditions of flow; second, they are implicated in an autoinhibitory mechanism in which ADAMTS13 adopts a closed, latent conformation, as outlined in section 1.4.2.

Earlier studies on the implication of C-terminal TSP1 and CUB domain deletions on VWF binding and proteolysis returned inconsistent results. Many studies show that ADAMTS13 lacking the C-terminal domains (MDTCS) can cleave full-length VWF and truncated portions of the VWF A2 domain under static conditions with similar or better efficacy than full-length ADAMTS13. However, MDTCS is shown to be less effective than full-length ADAMTS13 at cleaving full-length VWF multimers under flow and *in vivo*. This suggests that the CUB domains are not required for VWF proteolysis, but may be important for localizing ADAMTS13 to VWF under flow[56 57 62-66]. However, two studies found that MDTCS was equal to or more effective than full-length ADAMTS13 at cleaving multimeric VWF under flow[67 68]. This may be due to differences in assay conditions between studies; Feys *et al* used a closed system, creating shear in a PCR tube by using a vortexer to unravel VWF. This may reduce the need for MDTCS to dock to VWF for cleavage to occur, as they stay in proximity. Moreover, Tao *et al* use a low shear rate in a microfluidic flow system, while the CUB domains have been shown to be more important for binding VWF at higher shear rates[62].

Zanardelli *et al* performed binding and activity studies under both static and flow conditions using VWF and ADAMTS13 deletion mutants in an attempt to resolve conflicting evidence. They found that full-length ADAMTS13 TSP1-5 – 8 and CUB domains bind both globular and shear-unravelled VWF[69]. Feys *et al* found similar results, indicating that globular VWF-binding depends on C-terminal TSP1 and CUB domains of ADAMTS13 under flow[67]. Both studies conclude that the C-terminal domains are

responsible for binding to globular VWF in its D4-CK domains, forming circulating ADAMTS13-VWF complexes, and that this interaction alone is not proteolytic under shear. Shear stress is, however, required to unravel the VWF A2 domain and allow for subsequent proteolysis mediated by other ADAMTS13 domains as described in section 1.4.2[42].

The combination of these studies suggests the following mechanism of VWF-binding by ADAMTS13 under physiological conditions. ADAMTS13-CUB1/2 binding to VWF-D4-CK localizes ADAMTS13 to globular or shear-elongated VWF under flow. When sufficient shear forces unravel the A2 domain of VWF, ADAMTS13 is already in position to cleave VWF. The unfolding of the A2 domain is rather transient, as it unfolds and rapidly refolds[20 21], lowering the probability that A2 domain-specific binding sites present in MDTCS will be able to localize the scissile bond alone. Thus, prior docking of ADAMTS13 to VWF at a site outside of the A2 domain allows VWF cleavage to occur more readily under conditions of flow.

1.4.4 ADAMTS13 conformational dynamics

ADAMTS13 exists in both an "open" and a "closed" conformation. The closed conformation is an autoinhibited form in which the C-terminal TSP1 and CUB domains are bound to the spacer domain[70-74]. The binding of the ADAMTS13 spacer domain to VWF is an essential step for proteolysis[65], and this domain is shielded in closed conformation[74]. Upon binding of the CUB domains to the D4-CK domains of VWF as

previously described, the CUB-spacer interaction disassembles, exposing the spacer domain and allowing for ADAMTS13 to cleave shear-unravelled VWF[55]. This prediction is supported by a structural study using electron microscopy and small-angle x-ray scattering profiles of full-length ADAMTS13 and its truncated form MDTCS, which shows that full-length ADAMTS13 is in a folded state[71]. Furthermore, the linker regions within the 7 C-terminal TSP1-repeats of ADAMTS13 have been shown as essential to the flexibility of the ADAMTS13 C-terminal "tail", allowing the protease to adopt the closed conformation[70].

ADAMTS13 mutants have been explored in the context of conformational activation; notably, a gain-of-function ADAMTS13 mutant (GoF-ADAMTS13)[74], and a constitutively active ADAMTS13 mutant (caADAMTS13)[75] have been developed. GoF-ADAMTS13 contains mutations in the spacer domain (R568K/F592Y/R660K/Y661F/Y66F) and exhibits enhanced VWF A2 domain-cleaving activity *in vitro*, similar to truncated ADAMTS13 lacking the CUB domains[74 76 77] and WT ADAMTS13 following incubation with anti-CUB antibodies. These alterations are proposed to result in a proteolytically-enhanced form of ADAMTS13 due to its preferential adoption of the open conformation. A different approach was taken using caADAMTS13, which contains a mutation in the T8L region (A1144V), predicted to achieve open conformation by limiting linker flexibility[75]. caADAMTS13 showed enhanced cleavage of the VWF A2 domain *in vitro* compared to WT ADAMTS13 and GoF-ADAMTS13[75]. caADAMTS13 was also more effective than WT ADAMTS13 at

restoring blood flow in a distal $FeCl_3$-mediated middle cerebral artery occlusion (MCAo) model, and reduced tissue hypoperfusion in a transient MCAo model of ischemia/reperfusion injury[75]. However, this proposed mechanism has yet to be confirmed, and there are other potential regulatory mechanisms that remain to be explored.

1.5 Clinical significance of the ADAMTS13/VWF axis

Maintaining balance between VWF levels and ADAMTS13 activity is crucial to achieve hemostasis while avoiding thrombosis. Excess ultra-large VWF and/or insufficient ADAMTS13 activity can lead to excessive platelet-binding activity and is a risk factor for thrombosis. Insufficient VWF can lead to bleeding due to a lack of sufficient platelet-capture, or stabilization and recruitment of factor VIII.

1.5.1 Thrombotic thrombocytopenic purpura

Severe ADAMTS13 deficiency (<10%) can cause thrombotic thrombocytopenic purpura (TTP), a lethal, sometimes relapsing microvascular thrombotic condition with a mortality rate of 90% if untreated[78]. This condition is characterized by microangiopathic hemolytic anemia, thrombocytopenia, neurologic changes, fever, and renal insufficiency[79]. The pathophysiology of TTP is related to the circulation of ultra-large VWF[80], resulting from a lack of ADAMTS13 activity that would otherwise attenuate platelet capture by shortening hemostatically active VWF multimers[81]. Acquired TTP is an autoimmune condition and accounts for most TTP cases, wherein patients produce

autoantibodies that target ADAMTS13. Congenital TTP is an ultra-rare autosomal recessive condition caused by various mutations in the ADAMTS13-encoding gene, 9q34, resulting in low or no functional circulating ADAMTS13[81]. ADAMTS13 deficiency alone is believed to be insufficient to induce TTP – Furlan and Lämmle propose that a "triggering" event is required for TTP onset, such as pregnancy or infection, that causes activation or injury to the microvascular endothelium[79].

The current standard of treatment for TTP includes plasma exchange to remove autoantibodies (in the case of acquired TTP) and replenish ADAMTS13 levels. This may ameliorate symptoms, but does not necessarily resolve baseline ADAMTS13 deficiency and confers risk for other adverse effects associated with plasma exchange[82]. Additional treatments for acquired TTP include Caplacizumab, a humanized anti-VWF Nanobody® which binds the VWF A1 domain to prevent platelet-VWF binding and microthrombi formation[83]. Recombinant ADAMTS13 is undergoing clinical trials to treat acquired and congenital TTP (https://beta.clinicaltrials.gov/study/NCT03393975; https://beta.clinicaltrials.gov/study/NCT03922308)[84]. Finally, rituximab, an antibody that binds and depletes CD20-positive B cells, has been used to treat other autoimmune conditions and has shown promise for inducing long-term remission of acquired TTP[85 86].

1.5.2 von Willebrand's Disease

Insufficient functional VWF can lead to reduced platelet recruitment, resulting in a bleeding condition termed von Willebrand Disease (VWD)[87]. Bleeding associated with

VWD primarily occurs in the mucosa, causing symptoms including nose bleeds and menorrhagia[15]. There are multiple subtypes of VWD, with types 1 and 3 referring to quantitative defects, and type 2 to qualitatively abnormal VWF variants[88].

Type 1 VWD accounts for 60-80% of cases and refers to a partial quantitative deficiency of VWF[89]. It has been postulated that this subtype is primarily due to missense mutations in the VWF gene causing reduced VWF release into circulation[90 91]. Type 3 is the rarest form of VWD (<5% of all cases) and refers to a complete or nearly complete loss of circulating VWF. This subtype is also attributed to VWF gene mutations, including nonsense mutations, deletions, or defective alleles, causing incomplete expression and secretion of VWF[92]. Type 2 accounts for approximately 30% of cases, and can be further subcategorized into A, B, M, and N depending on the functional deficit. Type 2A, the most common of the 4 subtypes, refers to a relative loss in high- and intermediate- molecular weight multimers. This can occur from mutations causing impaired VWF dimerization or enhanced susceptibility to ADAMTS13 cleavage[93]. Type 2B results from gain-of-function mutations in the A1 domain of VWF that enhance platelet-binding, reducing circulating concentrations of high molecular weight VWF multimers and platelets[94]. Type 2M results from loss-of-function mutations in the A1 domain, diminishing platelet-binding ability[92]. Finally, Type 2N is caused by mutations in the D' and D3 domains that impair FVIII binding[88]. These individuals tend to have normal VWF multimer distribution and platelet-binding activity, but reduced circulating levels of FVIII[95]. Symptoms of Type 1 VWD, and some Type 2 patients (aside from 2B)

can be ameliorated with desmopressin, a pharmaceutical that enhances the release of VWF and FVIII[96]. Symptoms may also improve with recombinant VWF in some cases, including Type 3[96].

1.5.3 Significance of ADAMTS13 in other conditions

The importance of VWF regulation by ADAMTS13 in TTP and VWD is well-established. However, VWF and ADAMTS13 are now recognized as important contributors to a growing number of immunothrombotic conditions, including cancer, atherosclerosis, sepsis, Alzheimer's, and liver disease[97-102]. A pattern among these conditions is increased VWF levels due to endothelial dysfunction or activation, leading to VWF release. It is now known that VWF can interact either directly or in a platelet-dependent manner with not only platelets, but erythrocytes, sickle cell erythrocytes, lymphocytes, neutrophils, and deoxyribonucleic acid (DNA) contained in neutrophil extracellular traps (NETs)[103]. Recruitment and activation of these cells can amplify inflammation. For example, following injury, activated neutrophils can defend against pathogens by releasing serine proteases, generating reactive oxygen species, releasing inflammatory cytokines, and undergoing NETosis, releasing NETs[104]. However, these processes have the potential to inflict further tissue injury and contribute to overactivation of the immune system[105 106].

While recombinant ADAMTS13 infusion is currently undergoing clinical trials as a treatment for TTP, it has also been shown to improve outcomes in experimental models

of stroke[107 108], myocardial infarction[109], colitis[110], skin allograft[111], thrombotic microangiopathy[112], heparin-induced thrombocytopenia[113], renal disease[114], and trauma-induced organ failure[115]. These studies have not reported increased bleeding risk following recombinant ADAMTS13 administration, however this potential adverse effect requires further investigation.

1.5 Regulation of ADAMTS13

The regulation of ADAMTS13 is a topic still being explored, as this protease evades common regulatory mechanisms. Other metalloproteases, including other members of the ADAMTS family, can be inhibited by natural inhibitors found in blood, such as the tissue inhibitors of metalloproteinases (TIMPs) and α-2-macroglobulin[116]. However, ADAMTS13 is shown to be resistant to these inhibitors[117-119]. Moreover, many other coagulation proteases are secreted as a zymogen, requiring cleavage at specific peptide bond(s) by another protease to become activated. Interestingly, all known ADAMTS proteases require cleavage within their propeptide region to become catalytically active[120], with the exception of ADAMTS13 and possibly ADAMTS7[49 121 122]. Finally, ADAMTS13 has an unusually long circulating half-life of 2-7 days[123], exemplifying its stability in circulation.

While the shear-dependent availability of VWF and the closed conformation of ADAMTS13 help to limit its activity to sites of vessel injury, the question remains: how does VWF recruit platelets to the site of injury despite the presence of ADAMTS13,

which cleaves VWF at a similar shear rate required for platelet binding? It is possible that VWF-platelet string formation is simply governed by excess stoichiometry of VWF relative to ADAMTS13[124] combined with the mechanosensitive nature of VWF platelet-binding activity. However, this mechanism does not account for dynamic changes in VWF platelet-capturing activity in the early stages of clot development compared to later stages and would leave ADAMTS13 as possibly the only blood protease without a direct mechanism of regulation. Due to these unique qualities of ADAMTS13, exploration of novel regulatory mechanisms has been required.

1.6 Proteolytic regulation of ADAMTS13

Proteolytic degradation of ADAMTS13 may play a role in regulating its activity. Plasma obtained from sepsis-induced disseminated intravascular coagulation (DIC) patients[125] and an acute-phase acquired TTP patient with α2-antiplasmin deficiency[126] contains degraded forms of ADAMTS13. Neutrophil elastase levels were also shown to be negatively correlated with ADAMTS13 antigen and activity in the DIC patients[125]. Moreover, a case report demonstrated that α1-antitrypsin administration (the physiologic granulocyte elastase inhibitor) could help prevent the appearance of circulating ultra-large VWF multimers in a chronically relapsing TTP patient, however it did not fully prevent relapse[127]. This evidence suggests the potential impact of elastase- and plasmin-mediated ADAMTS13 cleavage on its activity *in vivo*, but whether this is a pathogenic mechanism in the onset or worsening of these conditions remains unclear.

Coagulation and fibrinolytic proteases including thrombin, plasmin, factor Xa, and factor XIa, and neutrophil elastase can cleave ADAMTS13 *in vitro*[126 128-130]. Cleavage of ADAMTS13 within the C-terminal tail removes the CUB domains, leaving proximal MDTCS mostly intact. Notably, plasmin can also cleave VWF, and increasing plasmin generation by infusing recombinant tissue plasminogen activator (tPA) has been shown to partially compensate for ADAMTS13 deficiency in a mouse model of thrombotic microangiopathy[131]. However, endogenous plasmin generation is not sufficient to cleave VWF during acute episodes of TTP, suggesting this is not a significant mechanism of VWF regulation.

Crawley *et al.* demonstrated that thrombin- and plasmin-mediated cleavage of ADAMTS13 abolishes its activity toward purified human VWF under static conditions *in vitro*[128]. Garland *et al.* observed that ADAMTS13 degraded by thrombin and factor XIa exhibits enhanced cleavage of FRETS-VWF73 substrate, likely by relieving the closed conformation. Degradation by plasmin abolishes this activity, which is likely due to disruption of proximal exosites. However, ADAMTS13 degraded by thrombin, plasmin, or factor XIa has an impaired ability to cleave VWF-platelet strings on the surface of endothelial cells under conditions of flow[129]. These observations are consistent with several *in vivo* studies showing that the ADAMTS13 CUB domains facilitate binding of VWF under flow. Banno *et al.* found that mice expressing ADAMTS13 lacking domains C-terminal to TSP1-6 have accelerated ferric chloride-induced thrombus growth[62]. Similarly, De Maeyer *et al.* found that removal of the CUB domains abolishes proteolysis of intravital

VWF-platelet strings by 3-fold. Interestingly, additional removal of the 2 C-terminal TSP1 domains partially restored proteolysis, suggesting that the distal TSP1 domains may negatively regulate ADAMTS13 activity[63]. These studies suggest that the specific site at which ADAMTS13 is cleaved within the C-terminal tail may influence the effect of proteolytic modification on its activity. Thus, it is important to determine the sites within ADAMTS13 at which these proteases cleave, and whether their specific cleavage meaningfully impacts the activity of ADAMTS13 *in vivo*.

This proposed regulatory mechanism relies on local, transient physiological conditions at sites of vascular injury and in disease states, thus it is difficult to replicate *in vitro*. While evidence shows that endogenous ADAMTS13 is not proteolyzed in plasma following initiation of coagulation at its circulating concentration (~5 nM)[132], activating endogenous plasminogen in plasma with either streptokinase or uPA does result in endogenous ADAMTS13 degradation and impairs VWF multimer-cleaving activity to ~10% *in vitro*[133]. Moreover, cleavage of ADAMTS13 is concentration-dependent[126 128 129 132 133]. Thus, while systemic degradation of circulating ADAMTS13 may not represent a significant regulatory mechanism, ADAMTS13 activity may be attenuated by proteolysis locally at sites of vascular injury or in disease states, when protease concentrations are increased, or upon administration of supraphysiological concentrations of recombinant ADAMTS13 as a therapeutic. If proteolysis of infused recombinant ADAMTS13 occurs, preventing this may constitute a way to prolong or enhance its therapeutic efficacy. The significance of this mechanism has not yet been formally investigated *in vivo.* The

following work seeks to characterize protease-resistant mutants of ADAMTS13, which will be used to further clarify the physiological significance of proteolytic degradation of ADAMTS13.

2. PRELIMINARY DATA

Preliminary *in silico* and *in vitro* analysis of ADAMTS13, performed by Dr. Hasam Madarati as a part of his doctoral thesis, revealed two common potential site(s) of cleavage by various proteases: the T4L and T8L regions. Cleavage at these sites removes the C-terminal CUB domains from ADAMTS13 which are critical for binding VWF under flow. We have cloned and expressed 3 mutants of ADAMTS13: two mutants with one of each cleavage site mutated (T4L and T8L mutants), and a third with both sites mutated (T4L/T8L mutants). Mutations constitute replacement of the linker region(s) with a $(GGGS)_n$ linker of equivalent length.

3. HYPOTHESIS

Mutation of known cleavage sites within ADAMTS13 will produce a mutant that is resistant to degradation by various coagulation, fibrinolytic, and neutrophil proteases, without affecting its activity.

4. SPECIFIC AIMS

4.1 Characterize the ADAMTS13 mutants' resistance to degradation

Mutant resistance to purified proteases *in vitro* was characterized using western blot analysis. Commercial recombinant ADAMTS13 (crADAMTS13) was used as a control. This was performed to confirm whether the T4L and T8L regions and the I380 site are indeed the targets for cleavage of ADAMTS13, and whether mutation of these regions protect ADAMTS13 from degradation. Additionally, the degradation of crADAMTS13 and the resistance of the T4L/T8L and T4L/T8L + I380G mutants was measured in plasma coagulation and fibrinolysis assays, and in the presence of activated neutrophils.

4.2 Compare the proteolytic activity of the T4L/T8L mutant to WT ADAMTS13

A kinetic analysis of the T4L/T8L mutant was performed in comparison to crADAMTS13 using the FRETS-VWF73 assay. To replicate physiological conditions more closely, the microfluidic VWF cleavage assay was used to investigate the ability of the T4L/T8L mutant to cleave VWF under conditions of flow. This work has validated that the mutations do not negatively affect the enzyme's function.

4.3 Characterize a mutant with improved resistance to neutrophil elastase

To improve resistance to degradation in the presence of activated neutrophils, an additional cleavage site susceptible to neutrophil elastase was mutated. The mutant's

resistance to elastase was compared to the T4L/T8L mutant following incubation with purified elastase and activated neutrophils. This was performed to yield a potentially more potent antithrombotic for study in the context of thromboinflammation (e.g., sepsis).

5. MATERIALS AND METHODS

5.1 Protein preparation

5.1.1 ADAMTS13 mutant collection from stable cell lines

Frozen 1 mL stocks of human embryonic kidney (HEK) 293T cells (approximately 4.0 x 10^6 cells) expressing one of each ADAMTS13 mutant (T4L, T8L, T4L/T8L) and wild-type ADAMTS13 (WT), prepared by Dr. Hasam Madarati, were thawed and diluted in 9 mL of complete media (Dulbecco's Modified Eagle Medium [DMEM], 10% fetal bovine serum [FBS], 1% penicillin-streptomycin [Wisent: 450-201-EL]). See Appendix 1 for the amino acid sequence of WT, and the mutations pertaining to this work. Cells were pelleted at 500 xg for 5 minutes, then resuspended and plated in 10 cm dishes using 10 mL of complete media, prewarmed to 37°C. Plates were placed in an incubator set to 37°C and 5% CO_2, and the media was aspirated and replaced after 24 hours. At ~70% confluency, the media was aspirated and the cells were washed with 5 mL of Dulbecco's Phosphate-Buffered Saline buffer (DPBS; R&D Systems: B30050). The DPBS was aspirated and 1 mL of 0.25% trypsin-EDTA (Gibco: 25200-056) was added. After 5 minutes, 9 mL of complete media was added and the cells were collected and pelleted as described above. The cells were then resuspended and plated in 50 mL of

complete media in a T175 flask. At ~70% confluency, cells were pelleted as described above, then resuspended in 20 mL of complete media and placed in a roller bottle overnight at the lowest speed (0.5 rpm) to allow the cells to adhere. 230 mL of complete media was added to the bottle after 24 hours, and cells were grown for ~3 days at 1 rpm. Complete media was aspirated and cells were washed twice using 30 mL of DPBS. 250 mL of Gibco™ FreeStyle™ 293 Expression Medium (Thermo Scientific: 12338018) containing AEBSF (50 mg/L) was used for cell expression. The media was collected every 2 days for 3 to 6 collections per mutant, centrifuged at 4000 xg for 10 minutes, then filtered through a 0.45 µm filter and stored at -80°C.

5.1.2 ADAMTS13 mutant purification

Collected media was thawed overnight at 4°C and was then purified using Q Sepharose (Cytvia: 17051001) and HisPur Ni-NTA Resin (Thermo Scientific: 88221) according to the manufacturer's protocol.

Filtered media containing one of each mutant was diluted to a 2:1 volume ratio of Tris buffer (25 mM Tris, pH 8.0) to media. The column was set up with 5 mL resin bed volume of Q Sepharose beads. 2X bed volume of 0.1 M NaOH was passed through, followed by 2X bed volume of 0.1 M HCl, and finally, 5X bed volume of Tris buffer. The diluted media was loaded onto the column overnight at 4°C, and flowthrough was collected. The column was washed with 10X bed volume of Tris buffer, and the protein was eluted in ~1 mL fractions using 3X bed volume of Tris buffer containing 1 M NaCl

(pH 8.0). The eluted fractions were quantified using absorbance at 280 nm on the NanoDrop, and highly concentrated fractions were pooled together for Ni-NTA purification.

Pooled fractions were made to conditions like that of the wash buffer (25 mM Tris, 0.5 M NaCl, 10 mM imidazole, pH 8.0) for the Ni-NTA purification by diluting the NaCl concentration to 0.5 M using Tris buffer, adding imidazole to a concentration of 10 mM, followed by pH adjustment to 8.0. The column was set up with ~2 mL Ni-NTA resin bed volume and 10X bed volume of wash buffer was passed through. The media was then passed through, followed by a wash using 4X bed volume. The protein was then eluted in ~1 mL fractions using 12 mL of elution buffer (25 mM Tris-HCl, 0.5 M NaCl, 250 mM imidazole, pH 8.0). Fractions were then quantified and pooled as described above and concentrated using a centrifugal concentrator at 4000 xg for 10 to 60 minutes (molecular weight cut-off [MWCO] of 30 or 100 kDa). Samples were then incubated with 20 mM AEBSF to inhibit any contaminant serine proteases, followed by buffer exchange into ADAMTS13 reaction buffer (20 mM Tris-HCl, 150 mM NaCl, 10 mM $CaCl_2$, 10 μM $ZnCl_2$, 0.05% Tween-20, pH 7.4) using PD-10 desalting columns (GE Healthcare: 17-0851-01) as per the manufacturer's protocol. Final sample concentrations were measured using the Human ADAMTS13 Quantikine enzyme-linked immunosorbent assay (ELISA) Kit (R&D Systems: DADT160) as per the manufacturer's protocol.

5.1.3 ADAMTS13 mutant collection via transient transfection

Transient transfection of HEK 293T cells to express WT and the mutants were performed using the Transporter 5 reagent (Polysciences: 26008) according to the manufacturer's protocol. *E. coli* expressing plasmids containing either WT or mutant were prepared by Dr. Hasam Madarati. From these bacteria, the DNA to be used for transfection was isolated with a Maxi-Prep kit as per the manufacturer's protocol (Qiagen: 121123).

To prepare for transfection, HEK 293T cells were cultured in a T175 flask as previously described (section 5.1.1) until 50 – 70% confluency. 2 hours prior to transfection, the media was aspirated, the cells were washed with sterile PBS, and FreeStyle media was added. To prepare the DNA/Transporter 5 complexes for transfection, DNA (50 µg) was diluted in sterile transporter diluent (150 mM NaCl) followed by 200 µL Transporter 5 reagent (i.e., 4X DNA), to a final volume of 1/10th (5 mL) of the total cell culture volume (50 mL). The mixture was vortexed for 5 seconds, then incubated for 20 minutes at room temperature to allow the complexes to form. The mixture was then distributed evenly across the T175 flask containing the HEK 293T cells using a serological pipette, and the cells were placed in the incubator. 48 – 72 hours after transfection, the media was collected and stored in -80°C.

To prepare protein samples, collected media was thawed at 4°C and concentrated using centrifugal concentrators (MWCO of 30 or 100 kDa) at 4000 xg until the sample was approximately 1/100 of the original volume. Sample concentrations were determined using ELISA.

5.1.4 Total protein staining and western blot analysis of protein samples

Sodium dodecyl-sulfate polyacrylamide gel electrophoresis (SDS-PAGE) was used to separate protein samples under reducing conditions. Up to 15 μL (~2-5 μg) of protein sample was mixed with 4X Laemmli SDS-PAGE sample buffer (BioRad: 161-0747) containing 5% beta-mercaptoethanol and placed on a heating block at 95°C for 5 minutes. 8 μL of a protein marker (BioRad: 1610374) and the samples were loaded on a 4-20% SDS-PAGE gel (BioRad: 456-8086). The gel was electrophoresed in SDS-PAGE running buffer at 60 V for 12 minutes, then 200 V for 25 minutes. The gel was then set up for either total protein staining or western blotting to detect total or specific proteins, respectively.

Total protein staining was performed using SYPRO-Ruby (BioRad: 170-3125) according to the manufacturer's protocol to analyze the purity of the samples. The gel was washed twice with 15 mL of fixative buffer (40% methanol, 10% acetic acid) for 15 minutes each on a table-top shaker, then stained overnight using 15 mL of SYPRO-Ruby reagent covered from light. The gel was then washed twice with 15 mL of wash buffer (10% methanol, 7% acetic acid) for 15 minutes each. Imaging was performed using the ChemiDoc Imager System (Bio-Rad) and sample purity was obtained using the ImageLab Software v5.2.1 (Bio-Rad), indicated by the relative density of the band of interest to its associated lane.

Detection of specific proteins was performed using western blot. Protein was transferred from the gel to a nitrocellulose membrane using the Trans-Blot Turbo Transfer System (BioRad: 17001918). The membrane was then placed in a clean tray and blocked in 15 mL of block buffer (5% non-fat dry milk, Tris-buffered saline [TBS] with 0.01% Tween20 [TBST]) for 2 hours, or overnight at 4°C. The membrane was then rotated in a conical tube containing fresh block buffer with the primary antibody, affinity-purified rabbit anti-human ADAMTS13 (Abcam: ab28274), added at a dilution factor of 1/1000. This occurred for 2 hours at room temperature, or overnight at 4°C. The membrane was then washed three times with 15 mL of TBST wash buffer (TBS, 0.05% Tween20), then incubated with the secondary antibody, goat anti-rabbit horseradish peroxidase (HRP)-conjugated antibody, added at a dilution factor of 1/10000 for 1 hour as previously described. The membrane was then washed 6 times with 15 mL of TBST wash buffer, then placed on clear plastic wrap. HRP substrate solution (650 μL of Clarity peroxide reagent, 650 μL of Clarity luminol reagent [BioRad: 1705061]) was pipetted onto the membrane and left to incubate for 5 minutes covered from light. Imaging was performed on the ChemiDoc Imager System using the MultiChannel option on the ImageLab Software.

5.1.5 Developing the elastase-resistant ADAMTS13 mutant

The elastase cleavage site was identified[130] and mutated (I380G) using the Q5 Site-Directed Mutagenesis Kit (NEB: E0554S) according to the manufacturer's protocol. Primers were created using SeqBuilder 14 (DNASTAR Lasergene) and adjusted to avoid

possible hairpin structures and dimerization using the online OligoAnalyzer tool (Integrated DNA Technologies). The sequence of the resultant DNA vector was confirmed by the Mobix Lab (McMaster University). The vector was transiently transfected into HEK 293T cells, and expressed proteins were collected every 2 days in FreeStyle media (section 5.1.3). Media was concentrated using centrifugal filters (MWCO of 100 kDa), and the presence and integrity of protein was visualized using western blot (section 5.1.4).

5.2 ADAMTS13 mutant degradation assays

5.2.1 Purified protease experiments

In vitro proteolysis reactions of purified ADAMTS13 mutants (T4L, T8L, T4L/T8L, or T4L/T8L + I380G) or crADAMTS13 (R&D Systems: 6156-AD-020) as a control occurred in ADAMTS13 reaction buffer at a volume of 35 μL at 37°C. Each mutant or crADAMTS13 was incubated at a concentration of 50 nM, with various human recombinant proteases at 50 nM or 100 nM. Aliquots of 10 μL removed at 0, 30, and 180 minutes were stopped in 2 μL of 6X SDS-loading dye and separated via SDS-PAGE under reducing conditions, followed by western blotting (section 5.1.4).

5.2.2 Isolating neutrophils

To isolate neutrophils, blood was collected using five 2.7 mL BD vacutainer blood collection tubes containing sodium citrate (final 3.8%; Becton Dickinson: 363080). 10

mL of citrated blood was combined in a 15 mL conical tube, and 2.5 mL of 6% dextran in saline was added. The tube was mixed slowly 4 times in a figure 8 movement, then left to separate via red blood cell sedimentation for 45 minutes. The leukocyte-rich plasma layer was slowly removed and added to a clean tube using a pipette. In another 50 mL conical tube, room temperature Histopaque 1077 (Sigma: 10771) was added at an equal volume to that of the separated plasma layer. The plasma layer was then slowly added to the surface of the Histopaque without mixing. The plasma-Histopaque solution was centrifuged at 277 xg for 20 minutes with no deceleration. The supernatant was aspirated, and the pellet was slowly resuspended in 2.5 mL of ammonium-chloride-potassium lysing buffer (Gibco: A1049201), incubating for 4 minutes. Hank's Balanced Salt Solution (Gibco: 14065-056) was then added to a final volume of 50 mL and the solution was centrifuged at 277 xg for 5 minutes, at 4°C, with maximum acceleration and deceleration. The supernatant was aspirated and the pellet was slowly resuspended in 5 mL Roswell Park Memorial Institute (RPMI; Gibco: 11875093) media. The cells were counted using 0.4% trypan blue and a hemocytometer according to the manufacturer's protocol. The neutrophils were again pelleted, the supernatant was aspirated, and the pellet was resuspended at the desired concentration in RPMI.

For ADAMTS13 degradation assays, 0 – 500 x 10^3 neutrophils diluted in RPMI were activated using 100 nM phorbol myristate acetate (PMA) for 4 hours at 37°C, at a volume of 10 µL. A reaction containing 100 x 10^3 neutrophils without addition of PMA was also included. 50 nM WT, T4L/T8L, or T4L/T8L + I380G mutant were added to the

activated neutrophils to a final volume of 30 µL. The mixture was incubated for 1 hour at 37°C and protein degradation was visualized via western blot as previously described. Densitometric analysis was performed using ImageLab Software (BioRad) to compare full-length band volume of WT or mutant incubated with 50 x 10^3 activated neutrophils, relative to 0 activated neutrophils.

5.2.3 Plasma thrombin generation assay

In a black, round-bottom, 96-well plate, 3.33 µL of phosphatidylcholine-phosphatidylserine lipid vesicles (PCPS), prepared by Rida Malik of the Weitz Lab, was added to give a final concentration of 15 µM, followed by 36.6 µL of human platelet-poor plasma, and 10 µL of undiluted, 1:10, 1:100, or 1:1000 tissue factor (HemosIL RecombiPlasTin: 00020301400; concentration not provided by manufacturer) to HEPES buffer (20 mM HEPES), or 10 µL of HEPES buffer. The reaction was incubated at 37°C for 15 minutes. To initiate thrombin generation, 50 µL of substrate mixture (52 mM $CaCl_2$, 40 mM HEPES, 2 mM Z-Gly-Gly-Arg-AMC acetate [thrombin-specific fluorogenic substrate; MedChemExpress: HY-P0019A]) was added to the well, giving a final volume of 100 µL. An identical experiment was created in a separate plate without Z-Gly-Gly-Arg-AMC acetate, and with the addition of 200 nM crADAMTS13 and 1 mg/mL GPRP-amide to prevent fibrin formation and allow the removal of aliquots for western blot analysis. The reaction was read for 90 minutes in 1-minute intervals on kinetic fluorescence mode (excitation = 360 nm, emission = 460 nm) using the SpectraMax M3 plate reader and the SoftMax Pro v7.1.2 software (Molecular Devices).

Thrombin generation curves were generated using the Technothrombin® TGA Software (Technoclone, Vienna, Austria).

To measure crADAMTS13 degradation, aliquots were removed at 0, 10, and 90 minutes after initiating thrombin generation. Samples were separated via SDS-PAGE under reducing conditions, and western blotting for the metalloprotease domain of ADAMTS13 was performed (section 5.1.4).

5.2.4 Plasma fibrinolysis assay

In a clear, flat-bottom 96-well plate, 3 μL of 1 M $CaCl_2$ and 5 μL of 1:5 tissue factor were added to achieve final concentrations of 30 mM and 1:100, respectively. In a separate tube, 50 μL of human platelet-poor pooled plasma, activated tPA (Activase; obtained from the Jeffrey Weitz Lab) at 2, 6, or 10 nM, 120 nM of crADAMTS13 or T4L/T8L mutant, and HEPES-buffered saline (20 mM HEPES, 150 mM NaCl, pH 7.4) were combined. To examine crADAMTS13 and T4L/T8L degradation, an aliquot of this mixture was removed for the 0 timepoint. The mixture was then added to the plate to initiate the reaction at a final volume of 100 μL, and absorbance at 405 nm was read for the desired timeframe in 30-second intervals using the SpectraMax M2 plate reader and SoftMax Pro v7.0.3 software. An aliquot was removed for the final timepoint, and samples were separated via SDS-PAGE under reducing conditions. Western blot was performed for the M domain of ADAMTS13 to visualize degradation (section 5.1.4).

5.3 Characterizing T4L/T8L mutant activity

5.3.1 Kinetic analysis using FRETS-VWF73 assay

WT and mutant activity was characterized using the FRETS-VWF73 assay (AnaSpec: AS-63728-01)[134]. Reactions took place at 100 μL in a black, flat-bottom 96-well plate at 37°C. 20 nM purified T4L, T8L, and T4L/T8L was used. Alternatively, 20 nM WT and T4L/T8L protein derived from transient transfection of HEK 293T cells was used. Protein was incubated with 0 – 7.5 μM FRETS-VWF73 substrate diluted in FRETS buffer (20 mM Tris-HCl, 25 mM $CaCl_2$, 0.05% Tween-20, pH 7.4). Activity was measured using the SpectraMax M3 plate reader and the SoftMax Pro v5.4 software in kinetic fluorescence mode (excitation = 340 nm, emission = 450 nm). Fluorescence was measured every fifteen seconds for up to 4 hours. The initial rate of reaction was obtained using linear regression on data points from the beginning of the reaction ($R^2 > 0.8$). Using GraphPad Prism v8, nonlinear regression analysis of Michaelis Menten data was performed to obtain K_M, v_{max}, and k_{cat} values. A 2-way ANOVA with multiple comparisons was used on GraphPad Prism v8 to investigate statistically significant differences in initial rates (defined as $p < 0.05$).

5.3.2 Inhibition experiments

To determine whether the presence of contaminant proteins in the transient transfection-derived protein preparations may influence the results of the FRETS-VWF73 assay, the activity of the WT and T4L/T8L samples were first normalized to the activity

of 20 nM crADAMTS13 using 1 µM FRETS-VWF73 substrate as previously described (section 5.3.1). The corresponding volume (approximately 1 – 2 µL of each sample) was then preincubated with ADAMTS13 reaction buffer (no inhibitor), 1 mM AEBSF, 1 mM marimastat, or 0.5 M EDTA for 5 minutes at 37°C. FRETS-VWF73 substrate was then added to a final concentration of 1 µM to initiate the reaction. The initial reaction rates for WT and T4L/T8L were obtained as previously described (section 5.3.1), and the rates from each inhibitor condition were compared to the ADAMTS13 reaction buffer condition using 2-way ANOVA with multiple comparisons on GraphPad Prism v8. A statistically significant result was defined as $p < 0.05$.

5.3.3 HUVEC culture and seeding into flow channels

Human umbilical vein endothelial cells (HUVECs; Lonza: C2519A) were plated on 2% gelatin-coated 10 cm dishes in Endothelial Cell Growth Medium-2 BulletKit growth media (Lonza: CC-3162). Cells were placed in an incubator set to 37°C and 5% CO_2, and media was changed every 2 to 3 days until ~90% confluency.

For flow experiments, confluent HUVECs were seeded into an ibidi µ-Slide $VI^{0.4}$ (ibidi: 80606) according to the manufacturer's protocol. Each channel was coated at room temperature for 60 minutes using 30 µL of 75 µg/mL mouse collagen IV (R&D Systems: 3410-010-02) diluted in cold sterile 0.05 M HCl. HUVECs were trypsinized, pelleted at 500 xg for 5 minutes, and resuspended in growth media to a concentration of approximately 3 x 10^8 cells/mL. Excess collagen IV was washed from the channels using

cold DPBS, and 30 µL of cell suspension was added to each channel. The slide was placed in the incubator for 45 – 60 minutes to allow for adherence, then 60 µL of growth media was added to each well. Media was exchanged once daily until ~90% confluency prior to beginning the flow experiment.

5.3.4 Human washed platelet preparation

To wash platelets for use in the microfluidic VWF cleavage assay as described below, 8.5 mL of blood was collected into a BD Vacutainer blood collection tube containing 1.5 mL of anticoagulant acid citrate dextrose solution A (BD: 364606). The tube was centrifuged at 200 xg for 20 minutes at room temperature. The platelet-rich plasma (PRP) and buffy coat were gently transferred to a new tube, and 1.41 µL of 1 mg/mL prostaglandin I2 (PGI2; Cayman Chemical: 18220) was added for every 4 mL of PRP to prevent platelet activation. PRP was centrifuged at 1000 xg for 10 minutes to pellet platelets. Plasma was discarded and platelets were gently resuspended in 2X PRP volume of Tyrode's buffer (134 mM NaCl, 0.34 mM Na_2HPO_4, 2.9 mM KCl, 20 mM HEPES, 5 mM glucose, 0.35% bovine serum albumin, pH 7.0) and 0.12X Tyrode's buffer volume of acid citrate dextrose solution (ACD; 97.9 mM sodium citrate • $2H_2O$, 110 mM glucose, 78.1 mM citric acid • $2H_2O$). To prevent platelet activation, 0.706 µL of PGI2 for every 1 mL of final volume was added, resuspension was not performed until addition of ACD, and buffers were prewarmed to 37°C. The platelet solution was centrifuged at 1000 xg for 10 minutes, washed in 0.5X original PRP volume of Tyrode's buffer, and

were left to settle at room temperature for a minimum of 30 minutes. Experiments were performed within 5 hours.

5.3.5 Microfluidic VWF-platelet string cleavage assay

To prepare for the flow experiment, lyophilized platelets (Bio/Data Corporation: 101258) were reconstituted in manufacturer-provided TBS (200 000 cells/µL) and separated into one 2 mL aliquot per channel (i.e., experimental condition). Alternatively, washed platelets (see section 5.3.4) were prepared to the same approximate concentration. A 20 mM stock solution of $DiOC_6$, a green-fluorescent, lipophilic dye, was diluted to a 20 µM working stock in TBS. 100 µL of dye solution was added to each 2 mL aliquot of platelet solution to stain the platelets. 6 mL solutions of 5 nM MDTCS derived from transient transfection of HEK 293T cells (prepared by Peter Andrisani of the Colin Kretz Lab), 5 nM T4L/T8L mutant derived from transient transfection, or 5 nM purified WT were diluted in ADAMTS13 reaction buffer. The concentration of full-length WT in purified preparations was approximated to 5 nM based on western blot and ELISA concentration.

The experimental setup was assembled as outlined in Appendix 2 using a 30 mL syringe on a syringe pump, and the pump settings were adjusted to achieve the desired approximate shear rate as outlined in a chart provided by ibidi (https://ibidi.com/img/cms/support/AN/AN11_Shear_stress.pdf). The presence of VWF was confirmed by perfusing 2 mL of ADAMTS13 reaction buffer over a HUVEC-lined

channel, followed by 2 mL of either a 1:100 solution of polyclonal anti-VWF antibodies (Invitrogen: PA5-16634) to phosphate-buffered saline (PBS), or PBS alone. 3 mL of platelet solution was then perfused over the channel, and VWF-platelet string formation was monitored. Following perfusion of antibodies, no platelet strings were formed (Appendix 3), confirming that the observed platelet strings are formed due to VWF release.

To begin, channels were secured to the syringe pump and imaged one at a time, each corresponding to a different experimental condition. First, 2 mL of platelet solution is perfused over the channel to form stable VWF-platelet strings at a flow rate of 1 mL/min, followed by 2 mL of ADAMTS13 reaction buffer to wash the strings. Subsequently, at a flow rate of 2 mL/min, channels were perfused with 5 mL solution containing 5 nM WT, 5 nM MDTCS, 5 nM T4L/T8L mutant, or ADAMTS13 reaction buffer as a negative control. Channel imaging was initiated while channels were being perfused with wash buffer once the strings were brought into focus. Imaging continued for the remainder of the experiment until all fluid had perfused the channel to monitor VWF-platelet string cleavage.

A confocal microscope (Leica Stellaris 5 DMi8 automated, 11889014) was used on the STELLARIS 5 platform for imaging. The dye was set to FITC1 (excitation = 490 nm, emission = 525 nm), and a 10X dry lens was used. Videos were captured at 0.77 frames/sec at approximately the same channel region between experiments. The total length of VWF-platelet strings within the frame were quantified every 20 frames for 5

frames using the scale bar tool, ending at the final frame captured before the channel dried out. Using GraphPad Prism v8, these values were expressed as a percentage of the total length of VWF-platelet strings in the first quantified frame over time. A 2-way ANOVA with multiple comparisons was performed to measure differences between experimental conditions, with the exception of T4L/T8L due to a lack of replicates. A statistically significant result was defined as $p < 0.05$.

6. RESULTS

6.1 Protein preparation

6.1.1 Purified protein samples

Following protein purification using Q Sepharose and HisPur Ni-NTA columns, ADAMTS13 mutant protein concentration were determined using ELISA. Samples were separated via SDS-PAGE under reducing conditions using crADAMTS13 as a control. Gels underwent total protein staining using SYPRO-Ruby to analyze sample purity (Figure 5). The purity of each sample is represented by band density relative to overall lane density (%): crADAMTS13 = 75.35, T4L = 32.51, T8L = 20.91, and T4L/T8L = 21.67. Western blot was performed using an anti-ADAMTS13 M domain antibody (Figure 5). A single band was detected in each sample, corresponding to full-length protein.

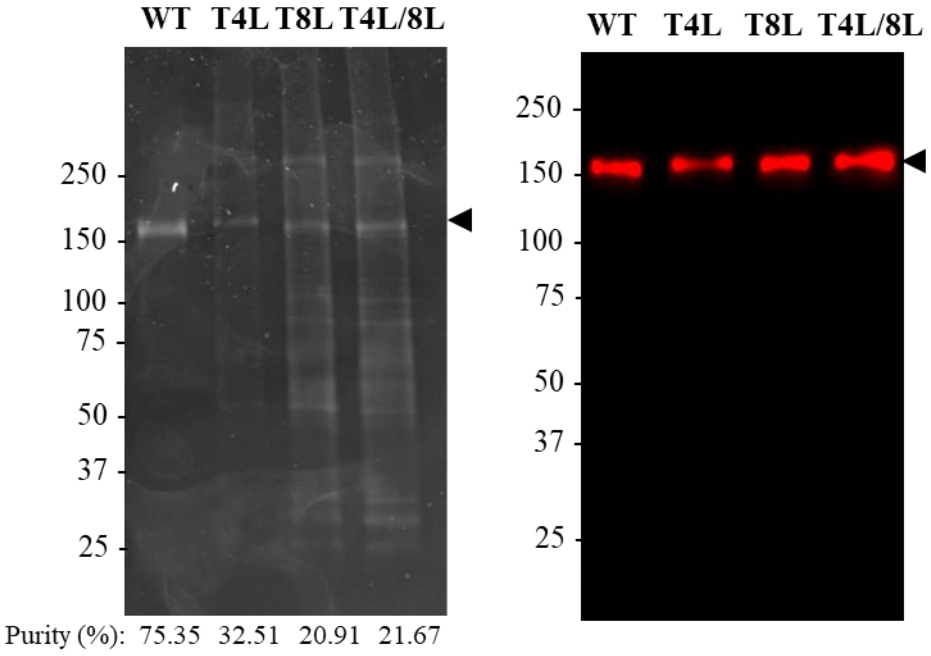

Figure 5. Purity analysis and western blot of ADAMTS13 mutant samples derived from stable cell lines. Purified and concentrated samples of ADAMTS13 mutants T4L, T8L, and T4L/T8L were separated via SDS-PAGE, with commercial recombinant ADAMTS13 (WT) as a control. Molecular weight references are indicated on the left (kDa). Bands at ~180 kDa correspond to full length protein, and are indicated with the black arrow. Left: total protein staining using SYPRO-Ruby was used to assess sample purity. The density (%) of each band corresponding to full length mutant relative to overall lane density was obtained using the Image Lab Software as a measure of sample purity: WT = 75.35%, T4L = 32.51%, T8L = 20.91%, T4L/T8L = 21.67%. Right: western blotting was used to verify the presence and integrity of specific protein using an anti-ADAMTS13 metalloprotease domain antibody.

6.1.2 Transient transfection-derived protein samples

Following approximately 100X concentration of media collected from transient transfected HEK293T cells containing WT, T4L, T8L, T4L/T8L, or T4L/T8L + I380G mutants using centrifugal filters (MWCO of 30 or 100 kDa), samples were separated via SDS-PAGE under reducing conditions. Western blot was used to visualize the presence

and integrity of protein (Figure 6A). An additional band, indicated by the red arrow, was repeatedly observed across transient transfection-derived samples and in human plasma alone (Figure 6B). This is presumed to be a result of non-specific antibody binding to other highly concentrated protein, possibly albumin, which is abundant in FBS used in cell culture media and in human plasma[135]. Some WT preparations were degraded, which did not occur in the mutant preparations.

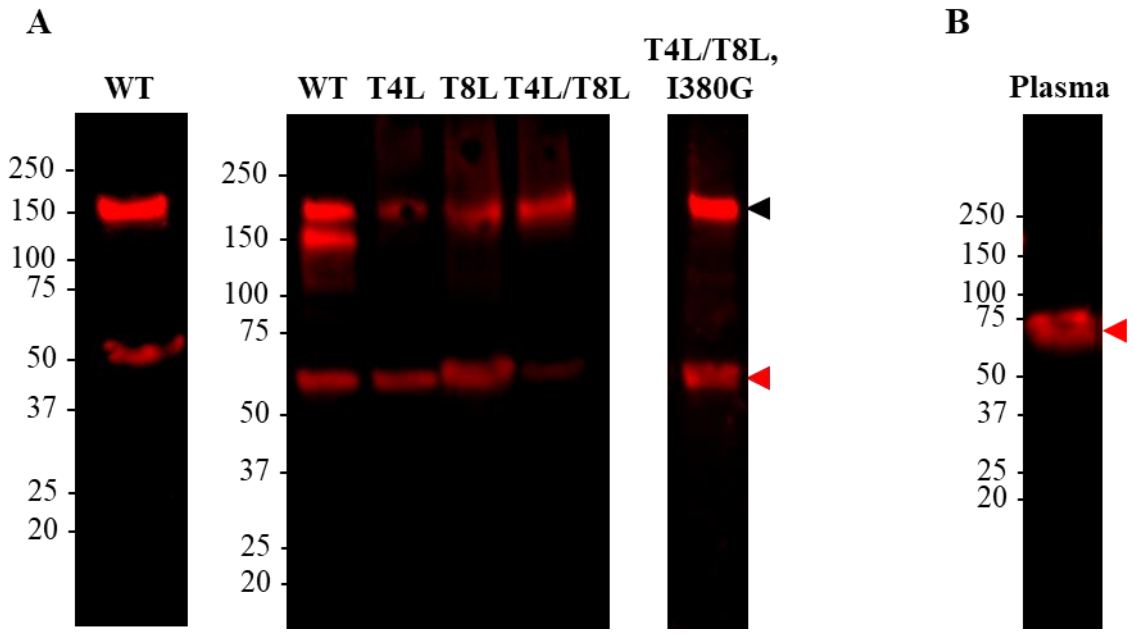

Figure 6. Western blot of WT and mutant ADAMTS13 samples derived from transient transfection of HEK 293T cells. Cell culture media was collected and concentrated approximately 100X using centrifugal filters (MWCO of 30 or 100 kDa). Samples of WT and T4L, T8L, T4L/T8L, or T4L/T8L + I380G mutants were separated via SDS-PAGE under reducing conditions. Presence and integrity of protein was visualized via western blot using a polyclonal anti-ADAMTS13 metalloprotease domain antibody. (A) Protein samples, with degraded and non-degraded preparation of WT. (B) Non-specific band in human plasma alone. Molecular weight references are indicated on the left (kDa). Bands at ~180 kDa correspond to full length protein and are indicated with the black arrows. Non-specific antibody binding is indicated by red arrows.

6.2 Resistance of ADAMTS13 mutants to degradation

6.2.1 Purified proteases

To examine whether the mutants are resistant to proteolysis by purified proteases, ADAMTS13 mutants were incubated at 50 nM with various proteases at 50 nM (plasmin, thrombin, kallikrein, and neutrophil-derived proteases cathepsin G, elastase, and proteinase 3) or 100 nM (factor XIa) for 0 to 180 minutes (Figure 7). crADAMTS13 was used as a control. Aliquots were removed at 0, 30, and 180 minutes, separated using SDS-PAGE under reducing conditions, and analyzed via western blotting using an anti-ADAMTS13 M domain antibody.

Coagulation proteases can cleave both T4L and T8L regions within ADAMTS13. Plasmin, thrombin, kallikrein, and factor XIa cleaved two sites in crADAMTS13 as is shown by the appearance of two M-domain containing cleavage products (Figure 7A). The T4L and T8L mutants were each protected from cleavage at one of these sites, given the appearance of only one product. The T4L/T8L mutant exhibits near-complete resistance to cleavage by plasmin, thrombin, factor XIa, and kallikrein over 180 minutes. When incubated with neutrophil-derived proteases elastase, cathepsin G, and proteinase 3, full-length crADAMTS13 is completely degraded by 30 minutes (Figure 7B). However, the T4L/T8L mutant exhibits partial resistance to degradation, as demonstrated by the persisting full-length band at 30 minutes. Additional cleavage sites are still present, as full-length T4L/T8L is fully degraded by 180 minutes by all three proteases. The

T4L/T8L + I380G mutant exhibited complete resistance to elastase over 180 minutes, suggesting the correct cleavage site was identified (Figure 7B).

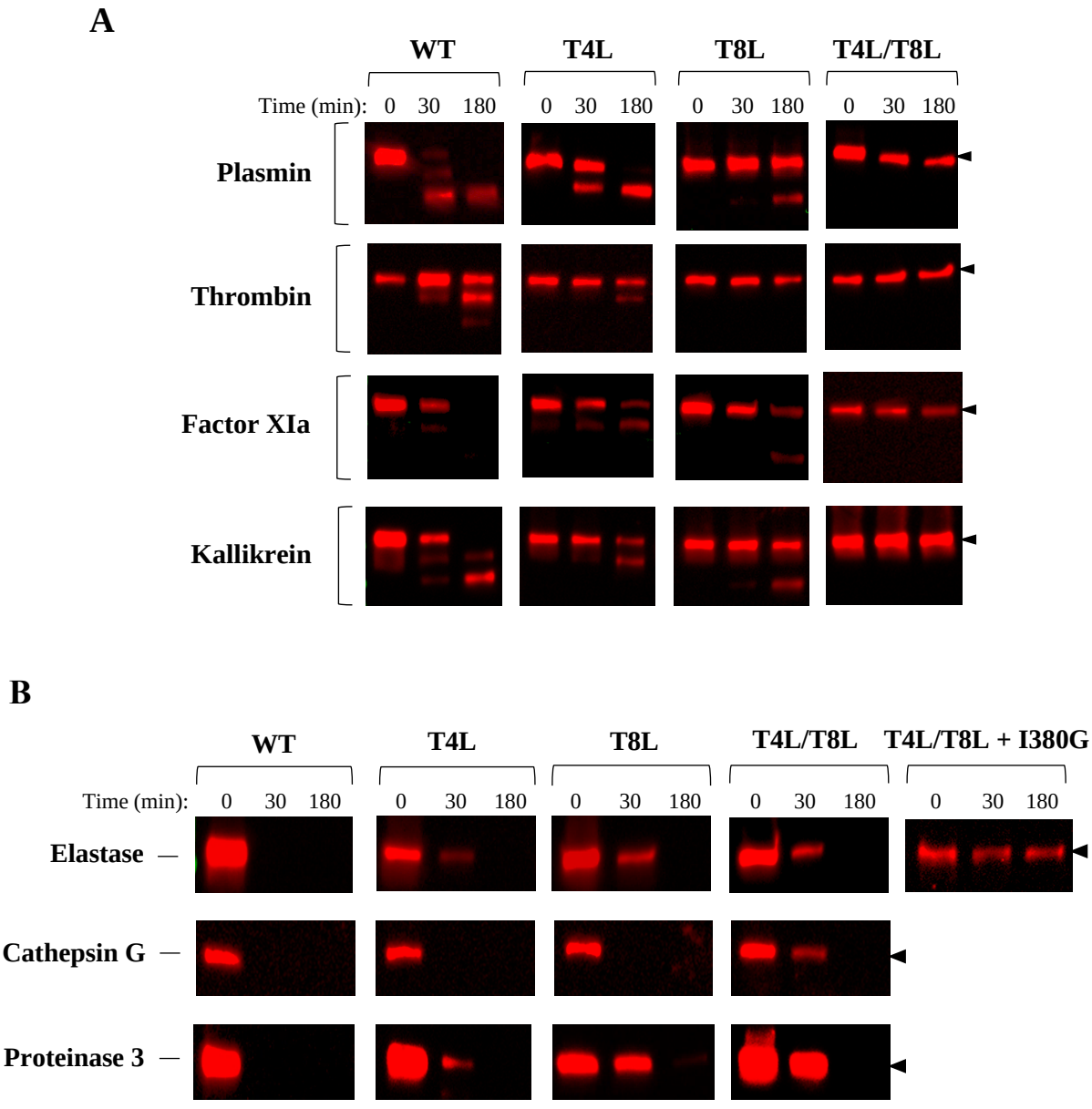

Figure 7. Characterizing the resistance of the ADAMTS13 mutants against proteolysis by purified proteases. ADAMTS13 mutants (T4L, T8L, and/or T4L/T8L) were incubated at 50 nM with purified (A) coagulation, fibrinolytic, and (B) neutrophil-derived proteases at 50 nM (plasmin, thrombin, kallikrein, elastase, proteinase 3, and cathepsin G) or

100nM (factor XIa) for 0 to 180 minutes. The T4L/T8L + I380G mutant with the predicted elastase cleavage site was also incubated with 50 nM elastase. Commercial recombinant ADAMTS13 (WT) was used as a control. Aliquots were removed at 0, 30, and 180 minutes, and separated via SDS-PAGE. Western blotting was performed using a polyclonal anti-ADAMTS13 metalloprotease domain antibody. The band corresponding to full-length protein (~180 kDa) is indicated by black arrows.

6.2.2 Activated neutrophils

To examine the resistance of the mutants to degradation in the presence of activated neutrophils, 50 nM WT, T4L/T8L, or T4L/T8L + I380G mutant was incubated with 0 – 50 x 10^3 activated neutrophils for 1 hour. Western blot was used to visualize degradation (Figure 8). Each protein exhibited varying degrees of degradation when incubated with 50 x 10^3 cells. Relative to the density of the full-length band in the presence of 0 cells, full-length WT exhibited the most significant degradation when incubated with 50 x 10^3 cells (10.0% remaining), followed by the T4L/T8L mutant (26.5% remaining), then the T4L/T8L + I380G mutant (71.5% remaining; Table 1). However, the T4L/T8L + I380G mutant was still fully degraded in the presence of 500 x 10^3 neutrophils, indicating that additional cleavage occurs in the presence of sufficient neutrophils (Figure 8).

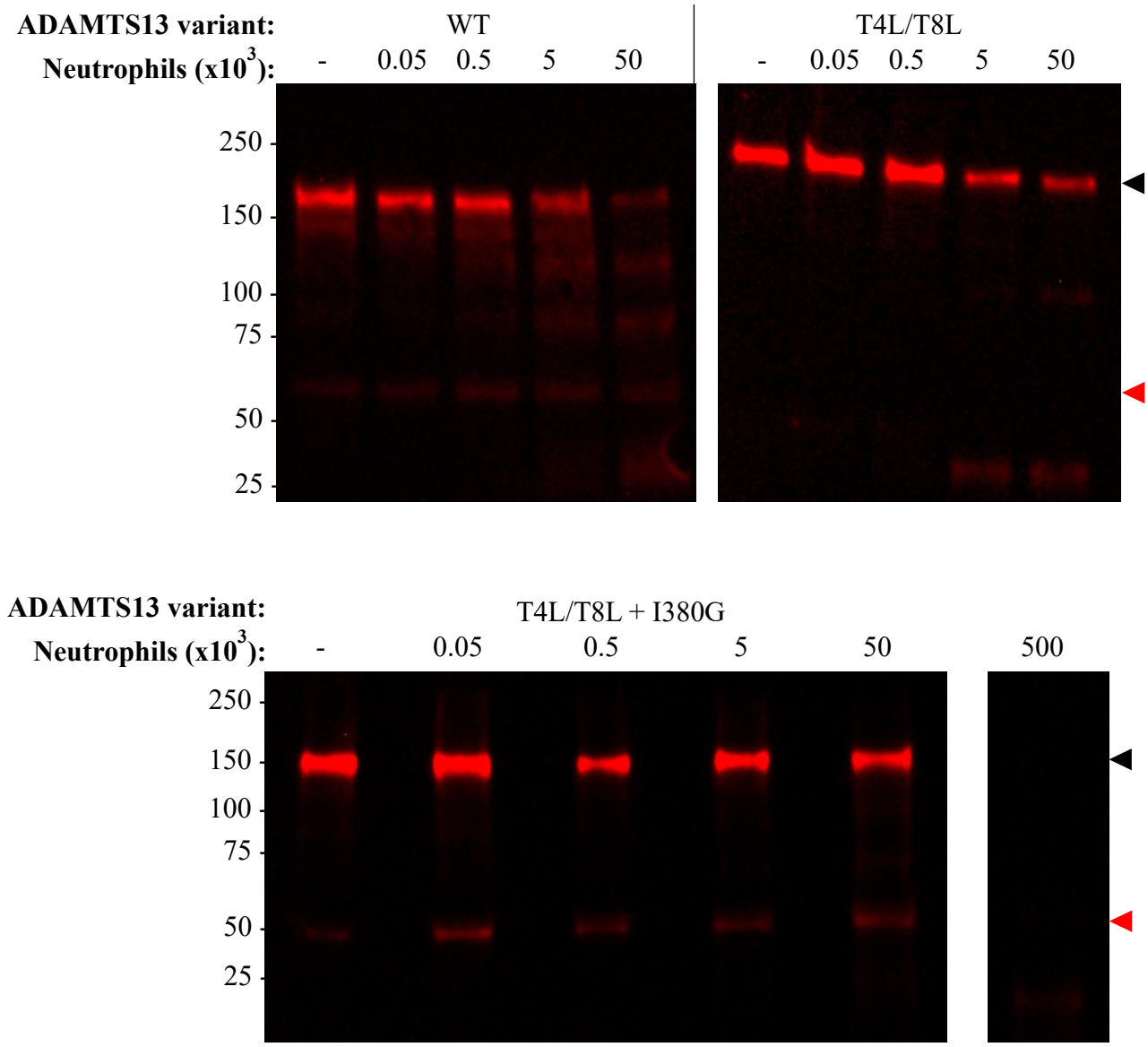

Figure 8. Resistance of ADAMTS13, T4L/T8L, and T4L/T8L + I380G mutants to activated neutrophils. 50 nM WT, T4L/T8L, or T4L/T8L + I380G mutant was incubated with 0 – 50 x 10^3 PMA-activated neutrophils, or 500 x 10^3 neutrophils as indicated. Reactions took place for 1 hour at 37°C, then samples were removed and separated via SDS-PAGE under reducing conditions. Cleavage was visualized with western blot using an anti-ADMATS13 metalloprotease domain antibody. Molecular weight references are indicated to the left (kDa). The level of full-length protein is indicated by black arrows, and the band corresponding to non-specific antibody binding is indicated by the red arrow.

Table 1. Resistance of ADAMTS13, T4L/T8L, and T4L/T8L + I380G mutants to 50 x 10^3 activated neutrophils. Data is expressed as a percent of total band signal volume following incubation with 50 x 10^3 activated neutrophils relative to incubation with 0 activated neutrophils.

Variant	% full-length
WT	10.0
T4L/T8L	26.5
T4L/T8L + I380G	71.5

6.2.3 Plasma coagulation and fibrinolysis

crADAMTS13 was added to plasma, then either coagulation (Figure 9) or coagulation and fibrinolysis (Figure 10) were initiated using varying concentrations of tissue factor (TF), or TF with varying concentrations of activated tPA, respectively. This was done to provide additional insight into the physiological relevance of ADAMTS13 cleavage by quantifying its degradation by proteases generated in plasma.

For the thrombin generation assay, human platelet-poor plasma was incubated with 200 nM crADAMTS13, varying dilutions of TF (1:10 – 1:10000; concentration not provided by manufacturer), 1 mg/mL GPRP-amide to prevent fibrin formation, and PCPS vesicles for 15 minutes. Coagulation was then initiated with calcium. Thrombin concentration was monitored in a parallel plate using a fluorogenic thrombin substrate (Figure 9A). Aliquots were removed prior to adding TF, and at 10 and 90 minutes following the addition of calcium, and crADAMTS13 cleavage was visualized via western blot (Figure 9B). In this assay, lower concentrations of TF lead to a relatively higher contribution of the intrinsic pathway (i.e., kallikrein, factor XIa, and factor XIIa) to

initial thrombin generation, whereas the extrinsic pathway dominates with higher TF concentrations[136]. However, regardless of TF concentration, crADAMTS13 was only minimally degraded after 90 minutes.

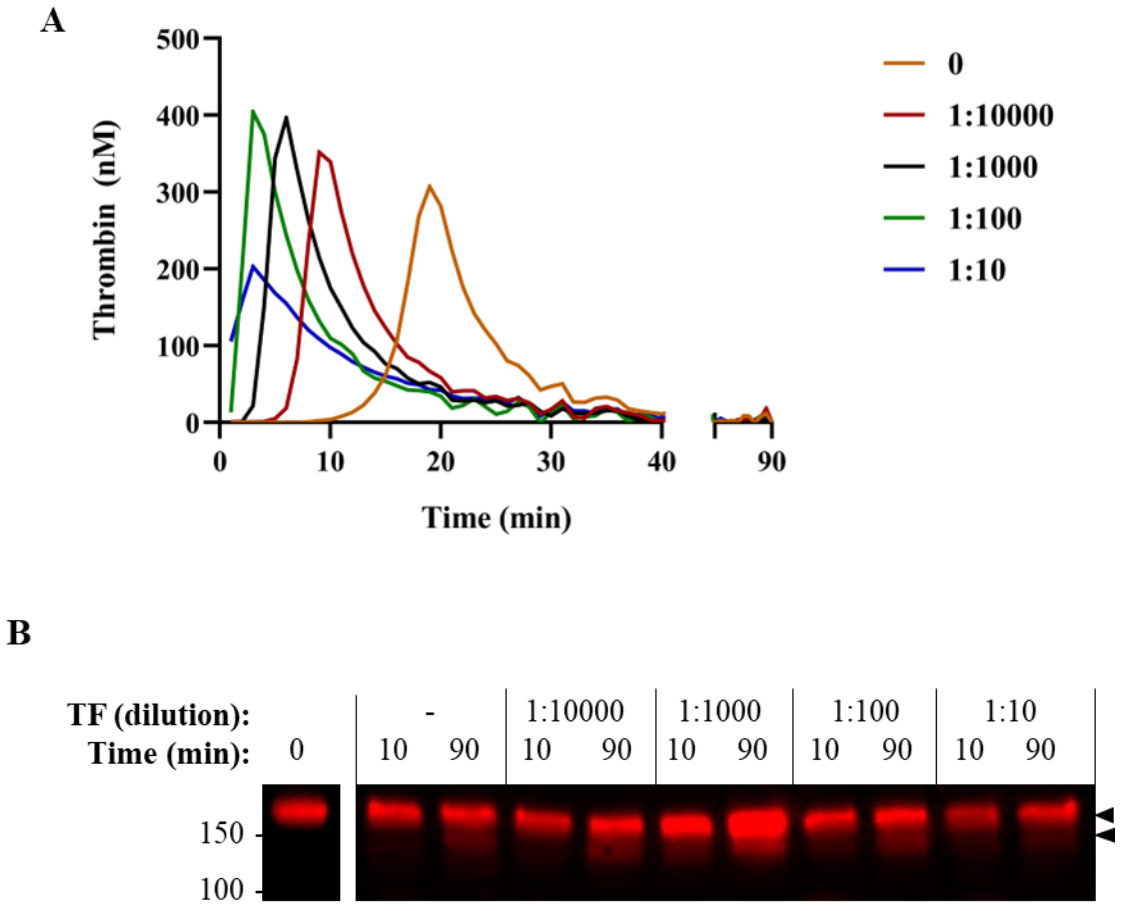

Figure 9. ADAMTS13 degradation in the plasma thrombin generation assay. Commercial recombinant ADAMTS13, varying dilutions of tissue factor (RecombiPlasTin; TF), and 1 mg/mL GPRP-amide were incubated in human platelet-poor plasma for 15 minutes. Thrombin generation was then initiated with $CaCl_2$ solution. (A) Thrombin concentration was quantified over time by measuring fluorescence (ex = 360 nm, em = 460) at 37°C, and curves were generated using the Technothrombin TGA Software. (B) Aliquots were removed prior to adding TF (0), and at 10 and 90 minutes after the addition of $CaCl_2$ solution. Samples were separated via SDS-PAGE under reducing conditions, and ADAMTS13

degradation was visualized via western blot using an anti-ADAMTS13 metalloprotease domain antibody. Molecular weight references are indicated on the left (kDa), and bands are indicated by black arrows.

Next, a plasma fibrinolysis assay was performed in the presence of 120 nM crADAMTS13 and 1:100 TF, across varying concentrations of tPA (2, 6, 10 nM) for 21 or 45 minutes (Figure 10). Fibrin formation and lysis was quantified by measured optical density (absorbance = 405 nm; Figure 10A). As demonstrated by western blot, crADAMTS13 degradation increased as tPA concentration was increased (Figure 10B). To examine the resistance of the T4L/T8L mutant under conditions of maximal crADAMTS13 degradation, the experiment was performed in the presence of 120 nM T4L/T8L mutant and 10 nM tPA for 45 minutes. The mutant exhibited complete resistance to degradation (Figure 10B).

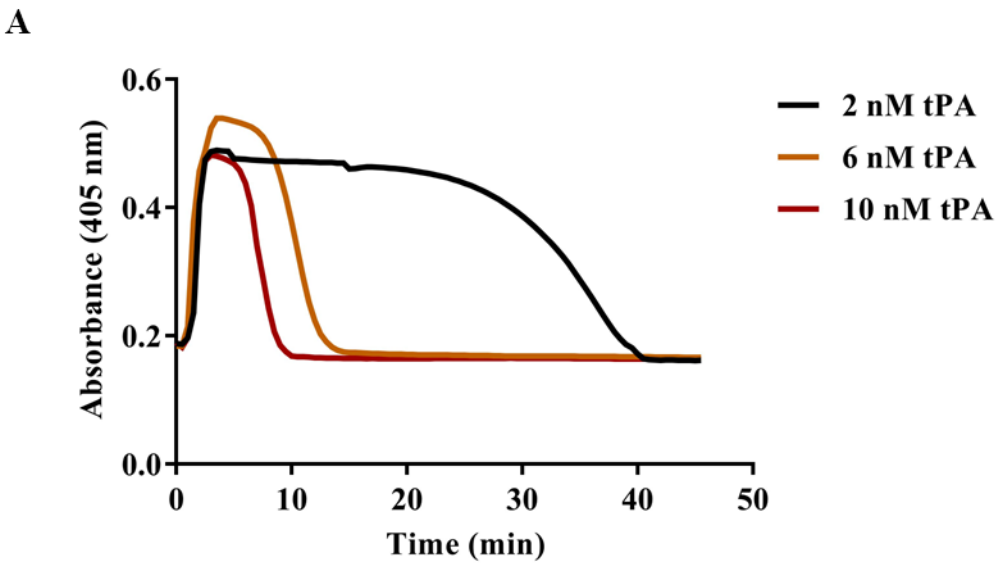

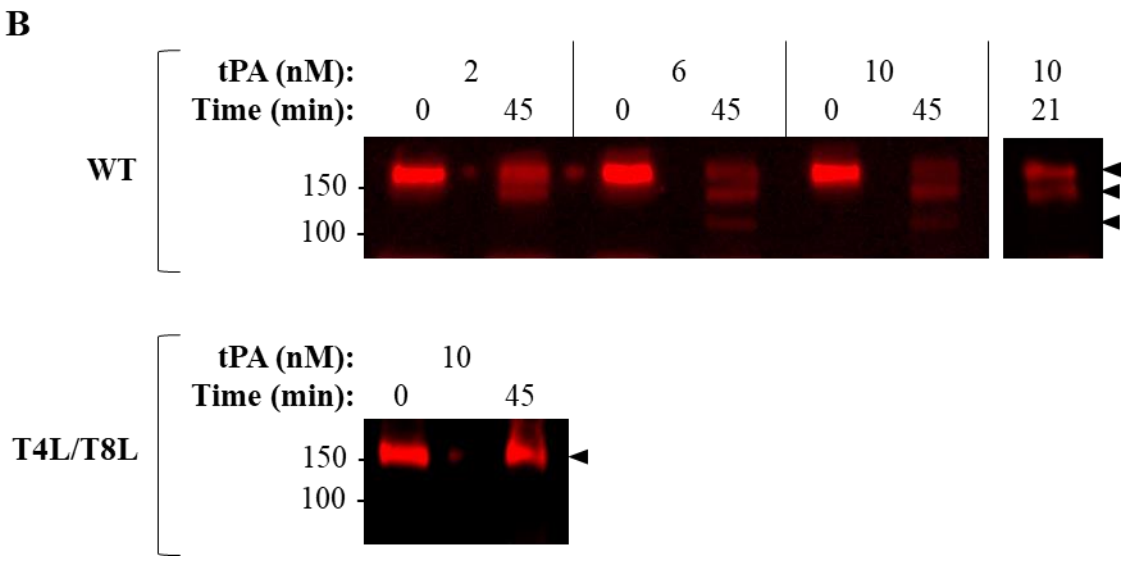

Figure 10. ADAMTS13 and T4L/T8L mutant degradation in the plasma fibrinolysis assay. Commercial recombinant ADAMTS13 (WT) or T4L/T8L mutant (120 nM) and varying concentrations of activated tissue-plasminogen activator (tPA) were added to human platelet-poor plasma. The plasma mixture was then added to a clear 96-well plate containing tissue factor and $CaCl_2$ solution. (A) Clot formation and lysis was quantified by measuring absorbance (405 nm) every 30 seconds. Absorbance increases with fibrin generation. (B) Aliquots were removed at the indicated time points, and samples were separated via SDS-PAGE under reducing conditions. Cleavage was visualized via western blot using an anti-ADAMTS13 metalloprotease domain antibody. Molecular weight references are indicated on the left (kDa), and bands are indicated by black arrows.

6.3 Proteolytic activity of ADAMTS13 mutants

6.3.1 Kinetic analysis of purified mutants using FRETS-VWF73

To determine whether the mutations affect the enzyme's kinetic parameters, the activity of purified T4L, T8L, and T4L/T8L was compared using the FRETS-VWF73 assay (n = 3; Figure 11). crADAMTS13 was used as a comparator. Differences may exist between in-lab purified WT ADAMTS13 and crADAMTS13, including purity, number of

freeze-thaw cycles, purification methodology, cell type used for protein expression, or other unknown factors. It is thus desirable to compare the mutants to WT that is prepared in-lab using the same methodology. However, all purified WT preparations throughout this work were degraded. Given the effect of conformational dynamics and fragmentation on activity (see section 1.4.4 and 1.6), these preparations were omitted from analysis. All three mutants and crADAMTS13 demonstrated a dose-dependent increase in the rate of reaction, and there were no significant differences between the initial rates produced by each enzyme ($p > 0.05$; Figure 11), except for T4L/T8L and T4L when incubated with 5 µM VWF73 ($p < 0.05$). K_M, v_{max}, and k_{cat} values are outlined in Table 2.

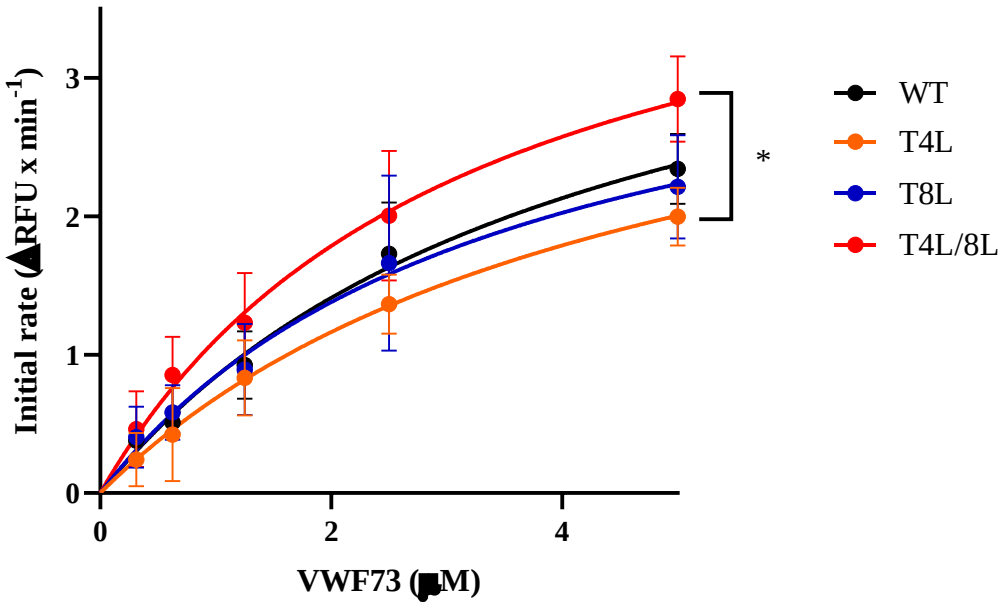

Figure 11. Michaelis-Menten analysis of purified T4L, T8L, and T4L/T8L mutants using the FRETS-VWF73 assay. 20 nM purified T4L, T8L, or T4L/T8L mutant was incubated with 0 - 5 µM FRETS-VWF73 substrate at 37°C (n = 2 – 3). Fluorescence was read every 15 seconds using a plate reader (ex = 340 nm, em = 450 nm). 20 nM commercial

recombinant ADAMTS13 (WT) was used as a comparator. Linear regression was performed on initial data points ($R^2 > 0.8$) to obtain initial reaction rates ($\Delta RFU \times min^{-1}$), and data were fitted to the Michaelis-Menten equation. Initial rates were compared using a 2-way ANOVA with multiple comparisons. $*p < 0.05$ at 5 µM VWF73

Table 2. Kinetic parameters, K_M, v_{max}, and k_{cat}, of purified T4L, T8L, T4L/T8L, and commercial recombinant ADAMTS13 (WT) using the FRETS-VWF73 assay. Values are expressed as mean ± SE.

Variant	K_M (µM)	v_{max} ($\Delta RFU \times min^{-1}$)	k_{cat} ($\Delta RFU \times min^{-1} \times \mu M^{-1}$)
WT	4.2 ± 1.3	4.4 ± 0.8	217.8 ± 38.6
T4L	4.7 ± 1.8	3.9 ± 0.9	193.7 ± 45.0
T8L	3.5 ± 1.8	3.8 ± 1.0	190.2 ± 51.7
T4L/T8L	3.2 ± 1.2	4.6 ± 0.9	230.8 ± 44.2

6.3.2 Troubleshooting the FRETS-VWF73 kinetic analysis assay using transient transfection-derived protein

To compare mutant activity to full-length WT prepared in-lab for future use in mouse models, transient transfection-derived protein was used, as degradation of WT had occurred throughout the purification process. The activity of WT was compared to T4L/T8L mutant using the FRETS-VWF73 assay (Figure 12). Concentrations were derived from ELISA, and the presence of protein was validated by western blot (see Figure 6). However, upon incubating 20 nM of these samples with 0 – 7.5 µM VWF73 substrate, the reaction rate was non-saturable, and Michaelis-Menten analysis produced a linear fit with ambiguous K_M and v_{max} calculations. In prior studies, the reaction rate begins to plateau at approximately 5 µM substrate[76 119]. Moreover, the slope of the line for T4L/T8L is approximately 1.5-fold higher than WT. This seemed to align with the volume required to achieve 20 nM of each sample as measured by ELISA (i.e., the

T4L/T8L sample had a lower concentration, and approximately 1.5X WT volume was pipetted into the reaction). Together, this suggests something else in the preparations was affecting the kinetic data.

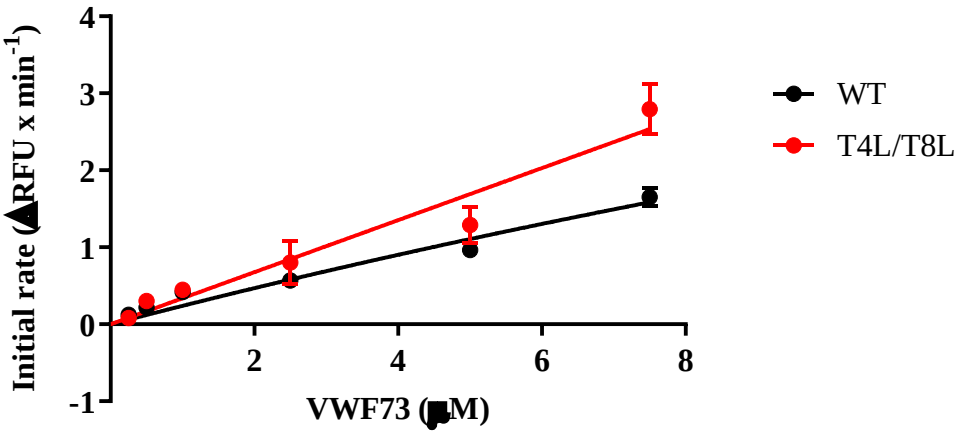

Figure 12. Michaelis-Menten analysis of transient transfection-derived ADAMTS13 and T4L/T8L mutant using the FRETS-VWF73 assay. 20 nM WT or T4L/T8L (as measured by ELISA) was incubated with 0 – 7.5 μM FRETS-VWF73 substrate at 37°C (n = 3). Fluorescence was read every 15 seconds using a plate reader (ex = 340 nm, em = 450 nm). Linear regression was performed on initial data points ($R^2 > 0.8$) to obtain initial reaction rates ($\Delta RFU \times min^{-1}$), and data were fitted to the Michaelis-Menten equation.

To determine whether it is a contaminant protease cleaving the VWF73 substrate, the activity of the transient transfection-derived samples was normalized to that of 20 nM crADAMTS13. The corresponding volume was then preincubated with either ADAMTS13 reaction buffer (no inhibitor), 1 mM AEBSF (serine protease inhibitor), 1mM marimastat (matrix metalloprotease inhibitor), or 0.5 M EDTA (broad-spectrum protease inhibitor via metal chelation) as a negative control (Figure 13). ADAMTS13 is resistant to AEBSF and marimastat, but not EDTA[119 126]. AEBSF and marimastat did not

significantly alter the rate of reaction in the presence of 1 μM FRETS-VWF73, whereas EDTA abolished activity ($p < 0.0001$). Given that the WT protein preparations are not exhibiting expected FRETS-VWF73 activity, troubleshooting is ongoing and efforts to purify full-length WT continue so it may be compared to purified T4L/T8L mutant.

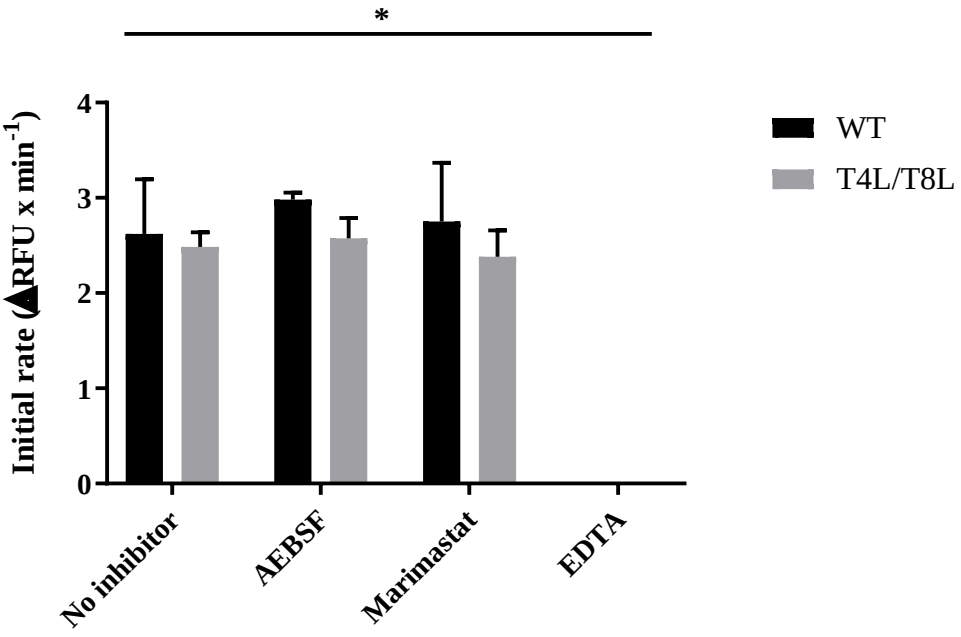

Figure 13. Effect of inhibitors on transient transfection-derived protein activity using the FRETS-VWF73 assay. The activity of WT and T4L/T8L mutant samples were normalized to that of 20 nM commercial recombinant ADAMTS13 using 1 μM FRETS-VWF73 substrate. The corresponding volume of each sample was then preincubated with ADAMTS13 reaction buffer (no inhibitor), 1 mM AEBSF, 1 mM marimastat, or 0.5 M EDTA for 5 minutes, and the reaction was initiated with 1 μM FRETS-VWF73 substrate (n = 3). Fluorescence was read every 15 seconds (ex = 340 nm, em = 450 nm). Linear regression was performed on initial data points ($R^2 > 0.8$) to obtain initial reaction rates (ΔRFU x min^{-1}). The rates from each inhibitor condition were compared to the no inhibitor condition using 2-way ANOVA with multiple comparisons. *$p < 0.0001$

6.3.3 Microfluidic VWF-platelet string cleavage

To determine whether the mutations affect the ability of the T4L/T8L mutant to cleave VWF under conditions of flow, a microfluidic flow assay was adapted from a published protocol[137] (see Appendix 2 for a schematic of the experimental setup). In brief, DiOC6-stained platelets were perfused over a microfluidic flow chamber lined with HUVECs, shear-activating the cells. Stable VWF-platelet strings formed that can be visualized using a confocal microscope (see Appendix 3). The channel was imaged over time while perfusing 5 nM WT (n = 5), 5 nM MDTCS (n = 2), 5 nM T4L/T8L mutant (n = 1), or ADAMTS13 reaction buffer (n = 3) over the channel (Figure 14). These values were expressed as a percentage of the total length of VWF-platelet strings in the first quantified frame, over time. There were no significant differences at any timepoint between MDTCS and buffer alone. However, WT contained a significantly reduced proportion of strings than MDTCS at the third, fourth, and fifth timepoint ($p > 0.05$). The T4L/T8L mutant seems to exhibit similar activity to WT, however replication is needed to determine statistical significance. Thus, it was excluded from statistical analysis. If WT and the T4L/T8L mutant indeed have similar activity, this suggests that the mutations do not significantly affect the VWF-cleaving activity of the T4L/T8L mutant under conditions of flow.

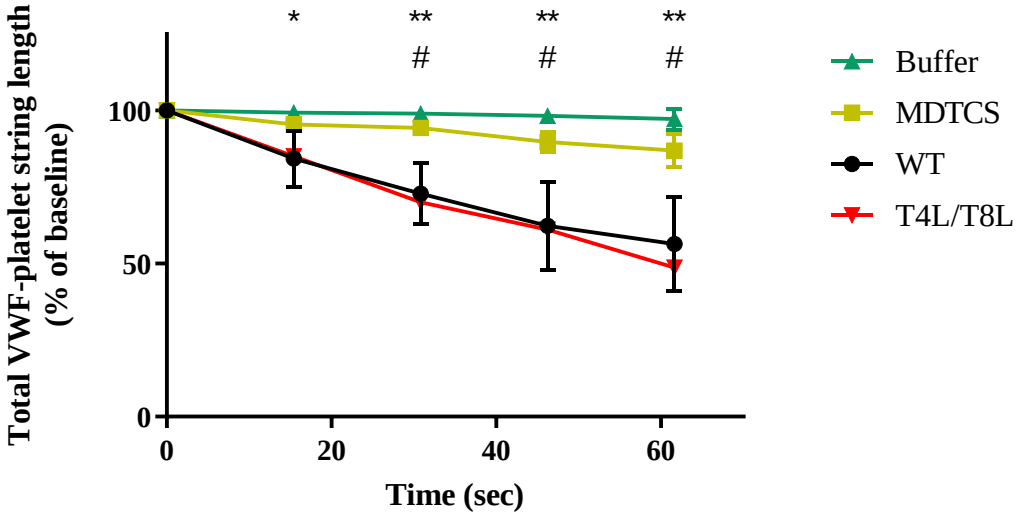

Figure 14. Activity of ADAMTS13, MDTCS, and the T4L/T8L mutant in a microfluidic flow assay. DiOC6-stained platelets were perfused over a microfluidic flow chamber lined with HUVECs, shear-activating the cells and forming VWF-platelet strings. Channels were then perfused with 5 mL of 5 nM WT (n = 5), 5 nM MDTCS (n = 2), 5 nM T4L/T8L mutant (n = 1), or ADAMTS13 reaction buffer (n = 3). Using a confocal microscope (10X dry lens; ex = 490 nm, em = 525 nm), videos were captured in a single frame at approximately the same channel region between experiments, at 0.77 frames/sec. The total length of strings within the frame was quantified every 20 frames for 5 frames, ending at the final frame captured before the channel dried out. Differences between groups at each timepoint were analyzed using a 2-way ANOVA with multiple comparisons, with the exception of T4L/T8L due to a lack of replicates. * = WT vs. Buffer, $p < 0.05$; ** = WT vs. Buffer, $p < 0.01$; # = WT vs. MDTCS, $p < 0.05$

7. DISCUSSION

This work characterized protease-resistant ADAMTS13 mutants, which may be used to investigate the importance of proteolytic degradation as a mechanism of ADAMTS13 regulation *in vivo*. *In silico* and *in vitro* analysis identified two regions within ADAMTS13 that are commonly cleaved by various proteases: the T4L and T8L regions. Replacing these regions with $(GGGS)_n$ linkers of equivalent length conferred

resistance to cleavage by plasmin, thrombin, factor XIa, and kallikrein, and partial resistance to neutrophil-derived proteases elastase, cathepsin G, and proteinase 3. Other cleavage sites were identified, including an elastase cleavage site in the D domain[130]. Neutrophil-derived proteases, which exhibit high promiscuity[104], may be an important contributor to ADAMTS13 degradation in thromboinflammatory conditions (e.g., sepsis)[125]. As described in section 1.6, the ADAMTS13-cleaving activity of elastase may be linked to sepsis-induced DIC and TTP[125 127]. Thus, this study also sought to improve the mutant's resistance to elastase. The new mutant (T4L/T8L + I380G) exhibited near complete resistance to purified elastase, and improved resistance to activated neutrophils relative to the T4L/T8L mutant. This may represent a more potent antithrombotic in the context of immunothrombosis. However, it is still fully degraded in the presence of 500 000 activated neutrophils, which may be attributable to the activity of proteinase 3 and cathepsin G. While this work investigates the most commonly- and rapidly-cleaved regions within ADAMTS13 among blood proteases, the relevance of other cleavage sites to its regulation will require further research.

While examining the degradation of crADAMTS13 in plasma, it was found that regardless of the concentration of TF used to initiate coagulation, which differentially implicates enzymes involved in the intrinsic and extrinsic pathways, crADAMTS13 was very minimally degraded in all conditions. This is despite thrombin reaching peak concentrations of approximately 400 nM, as measured by the parallel thrombin generation assay. This lack of proteolysis may be due to the presence of alternative, competing

thrombin substrates (i.e., fibrinogen). Lam *et al.* found that adding fibrinogen to purified crADAMTS13 incubated with thrombin could partially prevent its degradation[132]. However, this group also demonstrated that crADAMTS13 is cleaved significantly in the plasma coagulation assay, and that it could be prevented by adding a thrombin inhibitor (hirudin)[128]. The reason that this work could not replicate the published results remains unclear. Ultimately, the plasma coagulation assays within this work have shown that the presence of plasmin may be important *in vivo,* aligning with prior evidence[126 130].

The T4L and T8L regions have also been shown to be important to the flexibility of the C-terminal tail of ADAMTS13, allowing the protease to achieve closed conformation[86]. For this work, these regions were replaced with glycine-serine linkers in an attempt to maintain flexibility[138], but given the complex relationship between ADAMTS13 conformational dynamics and its proteolytic activity (see section 1.4.4), the activity of the T4L/T8L mutant was compared to WT. Using a microfluidic flow assay, this work showed that the T4L/T8L variant exhibits similar activity to WT under conditions of flow, however replication is needed to validate statistical significance. It was also shown that MDTCS was less effective than WT, and possibly the T4L/T8L mutant, at cleaving VWF-platelet strings, aligning with current literature outlining the importance of the C-terminal regions for docking to VWF under flow[62 67 129]. However, due to issues with protein preparation, replication of the T4L/T8L condition in the flow assay has been delayed (see section 6.3.2). Additionally, VWF-platelet string cleavage

data should be repeated with full-length WT and T4L/T8L protein samples prepared in the same manner to further validate the results.

The kinetic analysis performed with purified mutants showed no significant differences between initial reaction rates produced by the mutants and crADAMTS13, with the exception that T4L/T8L exhibited a significantly higher initial rate than T4L when incubated with 5 µM VWF73. While significance was not achieved in comparison to WT or T8L, their reaction rates did not differ from T4L. Thus, T4L/T8L activity may indeed be significantly higher if replication is performed, as only two were included for T4L/T8L due to limited protein. This improved reaction rate could be a result of the combined linker mutations inducing an open conformation, improving its activity under static conditions by exposing spacer domain exosites required for VWF cleavage[74]. The CUB domains normally bind to VWF C4-DK domains, which are not present on VWF73, to dissociate the closed conformation[42]. Numerous studies have shown that inducing open conformation by removing the C-terminal CUB domains or mutating residues involved in the spacer-CUB interaction can yield approximately 1.5 – 2.5-fold higher reaction rates in the FRETS-VWF73 assay[74 75 108 129]. Amino acid substitutions within the T8L region have been predicted to induce open conformation[75], however this remains to be confirmed. It is interesting to note that only the combination of mutations seems to improve activity, as the T4L and T8L mutants perform similarly to WT. It's been shown that deletion of any of the three distal linker regions (T2L, T4L, or T8L) induces a more preferential open conformation[70]. However, in this work, the T4L and T8L regions are replaced with

$(GGGS)_n$ linkers due to their flexibility, thus it is unclear whether conformation would be impacted by mutation of either linker. Conformational analysis is required to investigate this prediction, which may be achieved through atomic force microscopy[139], transmission electron microscopy[74], or immunoprecipitation using antibodies targeting residues that are cryptic in closed conformation[140].

It is crucial to purify intact WT in-lab for use as a comparator in mouse models. crADAMTS13 has higher purity at a higher concentration than in-lab preparations (see Figure 5). This could reduce the effects of contaminants that may impact enzyme activity or confound mouse study data. In addition, in-lab purified protein undergoes numerous freeze-thaw cycles, including after media collection, throughout purification, and after purification for use in the resistance experiments. This may affect the integrity of the protein via denaturation[141], a process that may not occur as frequently in the presumably optimized purification process used commercially. Moreover, differences in cellular processing of the protein, due to cell type or differences in the plasmid encoding the protein, may exist between in-lab ADAMTS13 and crADAMTS13. For example, HEK 293 cell-derived ADAMTS13 has a much lower half-life than Chinese hamster ovary cell (CHO)-derived ADAMTS13[108], which may be due to differences in glycosylation affecting clearance[50-52 130]. This variable has been shown to affect bleeding time in mice without affecting therapeutic efficacy[108]. Thus, it is essential to compare in-lab purified WT and mutants to limit these variables and determine whether it is solely the mutations that are responsible for differences in therapeutic efficacy or adverse outcomes.

It is both challenging and costly to produce and purify ADAMTS13 at high concentrations. Recent publications by other groups have been investigating ways to improve the yield of ADAMTS13 preparations, including optimizing the purification protocol[142] and altering the signal peptide to enhance expression[143]. Purified and transient transfection-derived preparations of WT obtained throughout this work were often degraded, and both the expression and the final yield of WT and mutant preparations were poor. However, the T4L, T8L, and T4L/T8L mutants were less susceptible to degradation (see Figure 6), suggesting that contaminant proteases in the protein preparations may be cleaving WT. Given that the T4L/T8L mutant exhibits similar activity to WT under flow (see Figure 12), this mutant may represent an alternative option for laboratory researchers seeking to purify ADAMTS13, as it may improve the yield of full-length protein. However, as stated previously, it is important to complete the kinetic characterization of the mutant to ensure the mutations do not affect its VWF-cleaving activity.

Given the limited literature on ADAMTS13 activity quantification using VWF released by HUVECs in a microfluidic chamber, the method used to quantify activity in this work is quite novel and may provide a way to calculate kinetic parameters under conditions of flow. However, it is important to consider the limitations of the flow assay and its qualitative nature. This work reported the total length of visible VWF-platelet strings in a given frame over time as a percentage of baseline. Variations in VWF release by HUVECs can affect many potential parameters of quantification. If strings are

connected to one another, or bind to multiple cells, one cleavage event may or may not clear the string from the frame, affecting whether total visible string length is reduced. Moreover, one long string can be cleaved at the proximal or distal end, drastically affecting the remaining length while undergoing only one cleavage event. Other ways to measure cleavage include quantifying the number of cleavage events, the average length of each platelet string, VWF-platelet string formation in the presence or absence of ADAMTS13, or measuring these parameters in randomly selected frames. Some of these methods have been used by other groups[129 137]. However, large variations in number, length, and multi-site binding of VWF-platelet strings between experiments are likely to confound these measurements. Thus, data was expressed as percent of baseline platelet-VWF string length over time to control for this, and a large frame was chosen to allow the visualization and quantification of many VWF-platelet strings.

ADAMTS13 is currently undergoing clinical trials for treatment of congenital and acquired TTP. Other preclinical studies have shown that ADAMTS13 may be an effective treatment for numerous other thromboinflammatory conditions[107-115]. Notably, this treatment does not seem to confer an increased bleeding risk[144-146], which is a limitation of current standard antithrombotic therapies including tPA, heparin, warfarin, and aspirin[147-149]. Supra-physiological doses of ADAMTS13 are used for therapeutic efficacy in animal models of myocardial infarction (3500 U/kg), acute ischemic stroke (3460 U/kg), and sepsis (3500 U/kg)[144-146], among others. In humans, however, the maximum dosage administered in clinical trials includes multiple intravenous infusions of 40 U/kg

ADAMTS13 over the course of weeks to treat an acute TTP episode, with or without standard plasma exchange[84]. This is the same dose provided for prophylaxis in congenital TTP, which brings stable circulating ADAMTS13 concentrations to a level that is normal in healthy individuals (~1 μg/mL)[84]. In preclinical TTP models, 40 U/kg provided the same therapeutic benefit as doses up to 200 U/kg (i.e., normalizing platelet, LDH, and schistocyte levels)[150]. Whether this dosage would be an effective therapeutic concentration for treatment of other conditions has not been investigated. TTP arises primarily from ADAMTS13 deficiency in conjunction with a triggering event, thus it is sensible that replenishing ADAMTS13 to normal levels is therapeutic. However, the ADAMTS13/VWF axis is implicated in numerous other conditions that arise from factors in addition to or separate from ADAMTS13 deficiency. A more potent ADAMTS13 mutant may help to reduce costs, alleviate the burden of receiving multiple infusions, and potentially improve therapeutic efficacy in TTP or other diseases.

tPA is the standard thrombolytic used to treat acute ischemic stroke, however it carries a high risk for intracerebral hemorrhage and there is a narrow time window in which therapeutic efficacy outweighs the risk of bleeding and other adverse outcomes[151]. In mouse models of ischemic stroke, ADAMTS13 administration has shown promise in dissolving VWF-rich thrombi without causing bleeding, reducing the neurotoxic effects of tPA when used in combination, and remaining effective over a larger time window than tPA[107 149 152 153]. tPA functions by activating plasmin for fibrinolysis, thus it is more effective against fibrin-rich thrombi and less effective towards VWF-rich thrombi[107].

Patient thrombi can vary in their relative composition of fibrin and VWF[107], and this is not readily measurable in an acute clinical scenario prior to administering treatment. Thus, combined ADAMTS13 and tPA therapy is a promising option that can target both VWF and fibrin, and reduce the concentration of tPA needed, limiting potential bleeding. However, this work shows that the plasminogen-activating activity of tPA causes crADAMTS13 degradation in plasma, which may occur locally when using ADAMTS13-tPA combination therapy *in vivo*. In addition, neutrophils are rapidly recruited to the site of infarction in ischemia-reperfusion injury and contribute to worsened outcomes[154]. This is attributed largely to VWF-neutrophil adhesion, and ADAMTS13 administration significantly reduces neutrophil recruitment in ischemia-reperfusion injury in mice[155]. Thus, given the resistance of the T4L/T8L +I380G mutant to plasmin and activated neutrophils, it may represent a more potent thrombolytic and anti-inflammatory agent than WT ADAMTS13 in the treatment of acute ischemic stroke. It may also further reduce the concentration of tPA required, reducing the risks associated with its use.

Sepsis is the body's overwhelming immune response to infection and is the most common cause of DIC. The pathogenesis of DIC is attributed to enhanced expression of TF due to excess pro-inflammatory cytokines, leading to widespread thrombin generation. Reduction in plasma antithrombin III[156], dysregulation of the protein C system[157], and insufficient TFPI function to compensate for TF pathway activation[158] exacerbate hypercoagulability. Fibrinolysis is also downregulated due to high levels of plasminogen activator inhibitor, type 1[159]. In addition to widespread microvascular thrombosis,

consumption of procoagulant factors and platelets can lead to bleeding. Deficiency of ADAMTS13 and excess high molecular-weight VWF multimers, due to widespread endothelial activation, is correlated with poorer outcomes in a variety of septic patient populations[125 160-162]. This suggests the potential therapeutic benefit of ADAMTS13 administration. Given that ADAMTS13 administration does not seem to cause bleeding, this may be a safer therapeutic option than targeting anticoagulants, coagulation factors, or plasmin. ADAMTS13 preferentially cleaves longer VWF multimers, which can help to prevent further platelet consumption and clear VWF-rich microthrombi in DIC, while also reducing VWF-mediated inflammation arising from neutrophil, platelet, and bacterial adhesion. VWF knockout and ADAMTS13 administration have been shown to improve outcomes and reduce microthrombi in animal models of sepsis. The evidence, however, is conflicting between models and the therapeutic efficacy of ADAMTS13 in sepsis requires further investigation[161 163 164]. Sepsis is characterized by massive activation and recruitment of immune cells, and cleavage of ADAMTS13 by neutrophil elastase may be linked to reduced ADAMTS13 activity in patients[125 127]. Given this, the T4L/T8L + I380G mutant, with resistance to neutrophil elastase and many coagulation factors that are upregulated in DIC, may represent a more potent therapeutic option than WT ADAMTS13.

Combining mutations investigated across multiple studies may produce a more potent therapy. Specific sets of mutations in the spacer domain of ADAMTS13 (R660K/F592Y/R568K/Y661F and R660K/F592Y/R568K/Y661F/Y665F) have shown to

confer resistance to binding of anti-ADAMTS13 antibodies found in patients with acquired TTP, while also inducing a preferentially open conformation that enhances antithrombotic activity *in vivo*[77 108]. Studying the mutants in this work *in vivo* may provide further insight into the importance of proteolytic degradation of ADAMTS13 as a physiological regulatory mechanism. If found to be a significant mechanism, combining the aforementioned mutations studied by other groups with the T4L, T8L, and I380G mutations that confer resistance to proteolytic degradation may improve therapeutic efficacy in acquired and congenital TTP, and in other conditions that may be ameliorated with ADAMTS13 administration.

8. FUTURE DIRECTIONS

Protein purification will undergo continued troubleshooting to finish characterizing the activity of the T4L/T8L and T4L/T8L + I380G mutants in comparison to WT, and produce comparable protein for use in mouse studies. Moreover, ADAMTS13 degradation has not been explored or quantified in animal models, despite evidence in humans. Thus, WT degradation and mutant resistance will be investigated via western blot using animal models of sepsis and in a TTP model, in conjunction with α2-antiplasmin and α1-antitrypsin administration. Finally, the therapeutic efficacy of the T4L/T8L and T4L/T8L + I380G mutants will be compared to WT in animal models of TTP, and in other disease models shown to be ameliorated by ADAMTS13 treatment (e.g., sepsis, myocardial infarction, acute ischemic stroke, deep vein thrombosis, etc.).

This work will determine the importance of ADAMTS13 cleavage to its therapeutic potential *in vivo*, and characterize a potential novel therapeutic for immunothrombosis.

9. REFERENCES

1. Galley HF, Webster NR. Physiology of the endothelium. *Br J Anaesth* 2004;93(1):105-13. doi: 10.1093/bja/aeh163 [published Online First: 2004/05/04]
2. Simionescu M, Antohe F. Functional ultrastructure of the vascular endothelium: changes in various pathologies. *Handb Exp Pharmacol* 2006(176 Pt 1):41-69. doi: 10.1007/3-540-32967-6_2 [published Online First: 2006/09/27]
3. Gale AJ. Continuing education course #2: current understanding of hemostasis. *Toxicol Pathol* 2011;39(1):273-80. doi: 10.1177/0192623310389474 [published Online First: 2010/12/02]
4. Andrews RK, Shen Y, Gardiner EE, et al. The glycoprotein Ib-IX-V complex in platelet adhesion and signaling. *Thromb Haemost* 1999;82(2):357-64. [published Online First: 1999/12/22]
5. Sixma JJ, van Zanten GH, Huizinga EG, et al. Platelet adhesion to collagen: an update. *Thromb Haemost* 1997;78(1):434-8. [published Online First: 1997/07/01]
6. Shida Y, Rydz N, Stegner D, et al. Analysis of the role of von Willebrand factor, platelet glycoprotein VI-, and alpha2beta1-mediated collagen binding in thrombus formation. *Blood* 2014;124(11):1799-807. doi: 10.1182/blood-2013-09-521484 [published Online First: 2014/07/24]
7. Li Z, Delaney MK, O'Brien KA, et al. Signaling during platelet adhesion and activation. *Arterioscler Thromb Vasc Biol* 2010;30(12):2341-9. doi: 10.1161/ATVBAHA.110.207522 [published Online First: 2010/11/13]
8. Loof TG, Deicke C, Medina E. The role of coagulation/fibrinolysis during Streptococcus pyogenes infection. *Front Cell Infect Microbiol* 2014;4:128. doi: 10.3389/fcimb.2014.00128 [published Online First: 2014/10/14]
9. Weisel JW, Litvinov RI. Mechanisms of fibrin polymerization and clinical implications. *Blood* 2013;121(10):1712-9. doi: 10.1182/blood-2012-09-306639 [published Online First: 2013/01/12]
10. Maas C, Oschatz C, Renne T. The plasma contact system 2.0. *Semin Thromb Hemost* 2011;37(4):375-81. doi: 10.1055/s-0031-1276586 [published Online First: 2011/08/02]
11. Revak SD, Cochrane CG, Griffin JH. The binding and cleavage characteristics of human Hageman factor during contact activation. A comparison of normal plasma with plasmas deficient in factor XI, prekallikrein, or high molecular weight kininogen. *J Clin Invest* 1977;59(6):1167-75. doi: 10.1172/JCI108741 [published Online First: 1977/06/01]
12. Crawley JT, Zanardelli S, Chion CK, et al. The central role of thrombin in hemostasis. *J Thromb Haemost* 2007;5 Suppl 1:95-101. doi: 10.1111/j.1538-7836.2007.02500.x [published Online First: 2007/08/01]
13. Cesarman-Maus G, Hajjar KA. Molecular mechanisms of fibrinolysis. *Br J Haematol* 2005;129(3):307-21. doi: 10.1111/j.1365-2141.2005.05444.x [published Online First: 2005/04/22]
14. Furlan M. Von Willebrand factor: molecular size and functional activity. *Ann Hematol* 1996;72(6):341-8. doi: 10.1007/s002770050184 [published Online First: 1996/06/01]
15. Sadler JE. Biochemistry and genetics of von Willebrand factor. *Annu Rev Biochem* 1998;67:395-424. doi: 10.1146/annurev.biochem.67.1.395 [published Online First: 1998/10/06]

16. Vlot AJ, Koppelman SJ, van den Berg MH, et al. The affinity and stoichiometry of binding of human factor VIII to von Willebrand factor. *Blood* 1995;85(11):3150-7. [published Online First: 1995/06/01]
17. Rand JH, Patel ND, Schwartz E, et al. 150-kD von Willebrand factor binding protein extracted from human vascular subendothelium is type VI collagen. *J Clin Invest* 1991;88(1):253-9. doi: 10.1172/JCI115285 [published Online First: 1991/07/01]
18. Sadler JE. Biomedicine. Contact--how platelets touch von Willebrand factor. *Science* 2002;297(5584):1128-9. doi: 10.1126/science.1075452 [published Online First: 2002/08/17]
19. Fujimura Y, Titani K, Holland LZ, et al. von Willebrand factor. A reduced and alkylated 52/48-kDa fragment beginning at amino acid residue 449 contains the domain interacting with platelet glycoprotein Ib. *J Biol Chem* 1986;261(1):381-5. [published Online First: 1986/01/05]
20. Meyer D, Girma JP. von Willebrand factor: structure and function. *Thromb Haemost* 1993;70(1):99-104. [published Online First: 1993/07/01]
21. Siedlecki CA, Lestini BJ, Kottke-Marchant KK, et al. Shear-dependent changes in the three-dimensional structure of human von Willebrand factor. *Blood* 1996;88(8):2939-50. [published Online First: 1996/10/15]
22. Nachman R, Levine R, Jaffe EA. Synthesis of factor VIII antigen by cultured guinea pig megakaryocytes. *J Clin Invest* 1977;60(4):914-21. doi: 10.1172/JCI108846 [published Online First: 1977/10/01]
23. Jaffe EA, Hoyer LW, Nachman RL. Synthesis of von Willebrand factor by cultured human endothelial cells. *Proc Natl Acad Sci U S A* 1974;71(5):1906-9. doi: 10.1073/pnas.71.5.1906 [published Online First: 1974/05/01]
24. Leebeek FW, Eikenboom JC. Von Willebrand's Disease. *N Engl J Med* 2016;375(21):2067-80. doi: 10.1056/NEJMra1601561 [published Online First: 2016/12/14]
25. Wagner DD, Olmsted JB, Marder VJ. Immunolocalization of von Willebrand protein in Weibel-Palade bodies of human endothelial cells. *J Cell Biol* 1982;95(1):355-60. doi: 10.1083/jcb.95.1.355 [published Online First: 1982/10/01]
26. Sporn LA, Marder VJ, Wagner DD. Inducible secretion of large, biologically potent von Willebrand factor multimers. *Cell* 1986;46(2):185-90. doi: 10.1016/0092-8674(86)90735-x [published Online First: 1986/07/18]
27. Wagner DD. Cell biology of von Willebrand factor. *Annu Rev Cell Biol* 1990;6:217-46. doi: 10.1146/annurev.cb.06.110190.001245 [published Online First: 1990/01/01]
28. Kanaji S, Fahs SA, Shi Q, et al. Contribution of platelet vs. endothelial VWF to platelet adhesion and hemostasis. *J Thromb Haemost* 2012;10(8):1646-52. doi: 10.1111/j.1538-7836.2012.04797.x [published Online First: 2012/05/31]
29. Stockschlaeder M, Schneppenheim R, Budde U. Update on von Willebrand factor multimers: focus on high-molecular-weight multimers and their role in hemostasis. *Blood Coagul Fibrinolysis* 2014;25(3):206-16. doi: 10.1097/MBC.0000000000000065 [published Online First: 2014/01/23]
30. Moake JL, Turner NA, Stathopoulos NA, et al. Involvement of large plasma von Willebrand factor (vWF) multimers and unusually large vWF forms derived from endothelial cells in shear stress-induced platelet aggregation. *J Clin Invest* 1986;78(6):1456-61. doi: 10.1172/JCI112736 [published Online First: 1986/12/01]

31. Savage B, Saldivar E, Ruggeri ZM. Initiation of platelet adhesion by arrest onto fibrinogen or translocation on von Willebrand factor. *Cell* 1996;84(2):289-97. doi: 10.1016/s0092-8674(00)80983-6 [published Online First: 1996/01/26]
32. Zhang C, Kelkar A, Neelamegham S. von Willebrand factor self-association is regulated by the shear-dependent unfolding of the A2 domain. *Blood Adv* 2019;3(7):957-68. doi: 10.1182/bloodadvances.2018030122 [published Online First: 2019/04/03]
33. Gogia S, Neelamegham S. Role of fluid shear stress in regulating VWF structure, function and related blood disorders. *Biorheology* 2015;52(5-6):319-35. doi: 10.3233/BIR-15061 [published Online First: 2015/11/26]
34. Pareti FI, Lattuada A, Bressi C, et al. Proteolysis of von Willebrand factor and shear stress-induced platelet aggregation in patients with aortic valve stenosis. *Circulation* 2000;102(11):1290-5. doi: 10.1161/01.cir.102.11.1290 [published Online First: 2000/09/12]
35. Plautz WE, Raval JS, Dyer MR, et al. ADAMTS13: origins, applications, and prospects. *Transfusion* 2018;58(10):2453-62. doi: 10.1111/trf.14804 [published Online First: 2018/09/13]
36. Furlan M, Robles R, Lammle B. Partial purification and characterization of a protease from human plasma cleaving von Willebrand factor to fragments produced by in vivo proteolysis. *Blood* 1996;87(10):4223-34. [published Online First: 1996/05/15]
37. Lynch CJ, Lane DA, Luken BM. Control of VWF A2 domain stability and ADAMTS13 access to the scissile bond of full-length VWF. *Blood* 2014;123(16):2585-92. doi: 10.1182/blood-2013-11-538173 [published Online First: 2014/02/22]
38. Springer TA. Biology and physics of von Willebrand factor concatamers. *J Thromb Haemost* 2011;9 Suppl 1:130-43. doi: 10.1111/j.1538-7836.2011.04320.x [published Online First: 2011/08/04]
39. Batlle J, Lopez-Fernandez MF, Lopez-Borrasca A, et al. Proteolytic degradation of von Willebrand factor after DDAVP administration in normal individuals. *Blood* 1987;70(1):173-6. [published Online First: 1987/07/01]
40. Zimmerman TS, Dent JA, Ruggeri ZM, et al. Subunit composition of plasma von Willebrand factor. Cleavage is present in normal individuals, increased in IIA and IIB von Willebrand disease, but minimal in variants with aberrant structure of individual oligomers (types IIC, IID, and IIE). *J Clin Invest* 1986;77(3):947-51. doi: 10.1172/JCI112394 [published Online First: 1986/03/01]
41. Zhang Q, Zhou YF, Zhang CZ, et al. Structural specializations of A2, a force-sensing domain in the ultralarge vascular protein von Willebrand factor. *Proc Natl Acad Sci U S A* 2009;106(23):9226-31. doi: 10.1073/pnas.0903679106 [published Online First: 2009/05/28]
42. Crawley JT, de Groot R, Xiang Y, et al. Unraveling the scissile bond: how ADAMTS13 recognizes and cleaves von Willebrand factor. *Blood* 2011;118(12):3212-21. doi: 10.1182/blood-2011-02-306597 [published Online First: 2011/07/01]
43. Huxley-Jones J, Clarke TK, Beck C, et al. The evolution of the vertebrate metzincins; insights from Ciona intestinalis and Danio rerio. *BMC Evol Biol* 2007;7:63. doi: 10.1186/1471-2148-7-63 [published Online First: 2007/04/19]
44. Zhou W, Inada M, Lee TP, et al. ADAMTS13 is expressed in hepatic stellate cells. *Lab Invest* 2005;85(6):780-8. doi: 10.1038/labinvest.3700275 [published Online First: 2005/04/05]

45. Tati R, Kristoffersson AC, Stahl AL, et al. Phenotypic expression of ADAMTS13 in glomerular endothelial cells. *PLoS One* 2011;6(6):e21587. doi: 10.1371/journal.pone.0021587 [published Online First: 2011/07/02]
46. Fujikawa K, Suzuki H, McMullen B, et al. Purification of human von Willebrand factor-cleaving protease and its identification as a new member of the metalloproteinase family. *Blood* 2001;98(6):1662-6. doi: 10.1182/blood.v98.6.1662 [published Online First: 2001/09/06]
47. Gerritsen HE, Robles R, Lammle B, et al. Partial amino acid sequence of purified von Willebrand factor-cleaving protease. *Blood* 2001;98(6):1654-61. doi: 10.1182/blood.v98.6.1654 [published Online First: 2001/09/06]
48. Zheng XL. Structure-function and regulation of ADAMTS-13 protease. *J Thromb Haemost* 2013;11 Suppl 1:11-23. doi: 10.1111/jth.12221 [published Online First: 2013/07/17]
49. Majerus EM, Zheng X, Tuley EA, et al. Cleavage of the ADAMTS13 propeptide is not required for protease activity. *J Biol Chem* 2003;278(47):46643-8. doi: 10.1074/jbc.M309872200 [published Online First: 2003/09/17]
50. Vanhoorelbeke K. Glycans of plasma ADAMTS13. *Blood* 2016;128(21):2485-86. doi: 10.1182/blood-2016-10-738773 [published Online First: 2016/11/26]
51. Verbij FC, Stokhuijzen E, Kaijen PH, et al. Identification of glycans on plasma-derived ADAMTS13. *Blood* 2016;128(21):e51-e58. doi: 10.1182/blood-2016-06-720912 [published Online First: 2016/08/31]
52. Zhou W, Tsai HM. N-Glycans of ADAMTS13 modulate its secretion and von Willebrand factor cleaving activity. *Blood* 2009;113(4):929-35. doi: 10.1182/blood-2008-07-167775 [published Online First: 2008/11/05]
53. Ricketts LM, Dlugosz M, Luther KB, et al. O-fucosylation is required for ADAMTS13 secretion. *J Biol Chem* 2007;282(23):17014-23. doi: 10.1074/jbc.M700317200 [published Online First: 2007/03/31]
54. Sorvillo N, Pos W, van den Berg LM, et al. The macrophage mannose receptor promotes uptake of ADAMTS13 by dendritic cells. *Blood* 2012;119(16):3828-35. doi: 10.1182/blood-2011-09-377754 [published Online First: 2012/02/01]
55. Petri A, Kim HJ, Xu Y, et al. Crystal structure and substrate-induced activation of ADAMTS13. *Nat Commun* 2019;10(1):3781. doi: 10.1038/s41467-019-11474-5 [published Online First: 2019/08/24]
56. Ai J, Smith P, Wang S, et al. The proximal carboxyl-terminal domains of ADAMTS13 determine substrate specificity and are all required for cleavage of von Willebrand factor. *J Biol Chem* 2005;280(33):29428-34. doi: 10.1074/jbc.M505513200 [published Online First: 2005/06/25]
57. Akiyama M, Takeda S, Kokame K, et al. Crystal structures of the noncatalytic domains of ADAMTS13 reveal multiple discontinuous exosites for von Willebrand factor. *Proc Natl Acad Sci U S A* 2009;106(46):19274-9. doi: 10.1073/pnas.0909755106 [published Online First: 2009/11/03]
58. Gao W, Anderson PJ, Sadler JE. Extensive contacts between ADAMTS13 exosites and von Willebrand factor domain A2 contribute to substrate specificity. *Blood* 2008;112(5):1713-9. doi: 10.1182/blood-2008-04-148759 [published Online First: 2008/05/22]
59. Soejima K, Matsumoto M, Kokame K, et al. ADAMTS-13 cysteine-rich/spacer domains are functionally essential for von Willebrand factor cleavage. *Blood* 2003;102(9):3232-7. doi: 10.1182/blood-2003-03-0908 [published Online First: 2003/07/19]

60. Pos W, Crawley JT, Fijnheer R, et al. An autoantibody epitope comprising residues R660, Y661, and Y665 in the ADAMTS13 spacer domain identifies a binding site for the A2 domain of VWF. *Blood* 2010;115(8):1640-9. doi: 10.1182/blood-2009-06-229203 [published Online First: 2009/12/25]
61. de Groot R, Bardhan A, Ramroop N, et al. Essential role of the disintegrin-like domain in ADAMTS13 function. *Blood* 2009;113(22):5609-16. doi: 10.1182/blood-2008-11-187914 [published Online First: 2009/02/24]
62. Banno F, Chauhan AK, Kokame K, et al. The distal carboxyl-terminal domains of ADAMTS13 are required for regulation of in vivo thrombus formation. *Blood* 2009;113(21):5323-9. doi: 10.1182/blood-2008-07-169359 [published Online First: 2008/12/26]
63. De Maeyer B, De Meyer SF, Feys HB, et al. The distal carboxyterminal domains of murine ADAMTS13 influence proteolysis of platelet-decorated VWF strings in vivo. *J Thromb Haemost* 2010;8(10):2305-12. doi: 10.1111/j.1538-7836.2010.04008.x [published Online First: 2010/08/11]
64. Zhang P, Pan W, Rux AH, et al. The cooperative activity between the carboxyl-terminal TSP1 repeats and the CUB domains of ADAMTS13 is crucial for recognition of von Willebrand factor under flow. *Blood* 2007;110(6):1887-94. doi: 10.1182/blood-2007-04-083329 [published Online First: 2007/06/02]
65. Zheng X, Nishio K, Majerus EM, et al. Cleavage of von Willebrand factor requires the spacer domain of the metalloprotease ADAMTS13. *J Biol Chem* 2003;278(32):30136-41. doi: 10.1074/jbc.M305331200 [published Online First: 2003/06/07]
66. Zhou W, Bouhassira EE, Tsai HM. An IAP retrotransposon in the mouse ADAMTS13 gene creates ADAMTS13 variant proteins that are less effective in cleaving von Willebrand factor multimers. *Blood* 2007;110(3):886-93. doi: 10.1182/blood-2007-01-070953 [published Online First: 2007/04/12]
67. Feys HB, Anderson PJ, Vanhoorelbeke K, et al. Multi-step binding of ADAMTS-13 to von Willebrand factor. *J Thromb Haemost* 2009;7(12):2088-95. doi: 10.1111/j.1538-7836.2009.03620.x [published Online First: 2009/09/22]
68. Tao Z, Wang Y, Choi H, et al. Cleavage of ultralarge multimers of von Willebrand factor by C-terminal-truncated mutants of ADAMTS-13 under flow. *Blood* 2005;106(1):141-3. doi: 10.1182/blood-2004-11-4188 [published Online First: 2005/03/19]
69. Zanardelli S, Chion AC, Groot E, et al. A novel binding site for ADAMTS13 constitutively exposed on the surface of globular VWF. *Blood* 2009;114(13):2819-28. doi: 10.1182/blood-2009-05-224915 [published Online First: 2009/07/10]
70. Deforche L, Roose E, Vandenbulcke A, et al. Linker regions and flexibility around the metalloprotease domain account for conformational activation of ADAMTS-13. *J Thromb Haemost* 2015;13(11):2063-75. doi: 10.1111/jth.13149 [published Online First: 2015/09/24]
71. Muia J, Zhu J, Gupta G, et al. Allosteric activation of ADAMTS13 by von Willebrand factor. *Proc Natl Acad Sci U S A* 2014;111(52):18584-9. doi: 10.1073/pnas.1413282112 [published Online First: 2014/12/17]
72. South K, Freitas MO, Lane DA. Conformational quiescence of ADAMTS-13 prevents proteolytic promiscuity. *J Thromb Haemost* 2016;14(10):2011-22. doi: 10.1111/jth.13445 [published Online First: 2016/10/28]
73. South K, Freitas MO, Lane DA. A model for the conformational activation of the structurally quiescent metalloprotease ADAMTS13 by von Willebrand factor. *J Biol Chem*

2017;292(14):5760-69. doi: 10.1074/jbc.M117.776732 [published Online First: 2017/02/18]
74. South K, Luken BM, Crawley JT, et al. Conformational activation of ADAMTS13. *Proc Natl Acad Sci U S A* 2014;111(52):18578-83. doi: 10.1073/pnas.1411979112 [published Online First: 2014/12/17]
75. South K, Saleh O, Lemarchand E, et al. Robust thrombolytic and anti-inflammatory action of a constitutively active ADAMTS13 variant in murine stroke models. *Blood* 2022;139(10):1575-87. doi: 10.1182/blood.2021012787 [published Online First: 2021/11/16]
76. Gao W, Anderson PJ, Majerus EM, et al. Exosite interactions contribute to tension-induced cleavage of von Willebrand factor by the antithrombotic ADAMTS13 metalloprotease. *Proc Natl Acad Sci U S A* 2006;103(50):19099-104. doi: 10.1073/pnas.0607264104 [published Online First: 2006/12/06]
77. Jian C, Xiao J, Gong L, et al. Gain-of-function ADAMTS13 variants that are resistant to autoantibodies against ADAMTS13 in patients with acquired thrombotic thrombocytopenic purpura. *Blood* 2012;119(16):3836-43. doi: 10.1182/blood-2011-12-399501 [published Online First: 2012/02/01]
78. Zheng X, Majerus EM, Sadler JE. ADAMTS13 and TTP. *Curr Opin Hematol* 2002;9(5):389-94. doi: 10.1097/00062752-200209000-00001 [published Online First: 2002/08/13]
79. Furlan M, Lammle B. Aetiology and pathogenesis of thrombotic thrombocytopenic purpura and haemolytic uraemic syndrome: the role of von Willebrand factor-cleaving protease. *Best Pract Res Clin Haematol* 2001;14(2):437-54. doi: 10.1053/beha.2001.0142 [published Online First: 2001/11/01]
80. Furlan M, Lammle B. von Willebrand factor in thrombotic thrombocytopenic purpura. *Thromb Haemost* 1999;82(2):592-600. [published Online First: 1999/12/22]
81. Levy GG, Nichols WC, Lian EC, et al. Mutations in a member of the ADAMTS gene family cause thrombotic thrombocytopenic purpura. *Nature* 2001;413(6855):488-94. doi: 10.1038/35097008 [published Online First: 2001/10/05]
82. Rock GA, Shumak KH, Buskard NA, et al. Comparison of plasma exchange with plasma infusion in the treatment of thrombotic thrombocytopenic purpura. Canadian Apheresis Study Group. *N Engl J Med* 1991;325(6):393-7. doi: 10.1056/NEJM199108083250604 [published Online First: 1991/08/08]
83. Scully M, Cataland SR, Peyvandi F, et al. Caplacizumab Treatment for Acquired Thrombotic Thrombocytopenic Purpura. *N Engl J Med* 2019;380(4):335-46. doi: 10.1056/NEJMoa1806311 [published Online First: 2019/01/10]
84. Scully M, Knobl P, Kentouche K, et al. Recombinant ADAMTS-13: first-in-human pharmacokinetics and safety in congenital thrombotic thrombocytopenic purpura. *Blood* 2017;130(19):2055-63. doi: 10.1182/blood-2017-06-788026 [published Online First: 2017/09/16]
85. Ahmad A, Aggarwal A, Sharma D, et al. Rituximab for treatment of refractory/relapsing thrombotic thrombocytopenic purpura (TTP). *Am J Hematol* 2004;77(2):171-6. doi: 10.1002/ajh.20166 [published Online First: 2004/09/25]
86. Fakhouri F, Vernant JP, Veyradier A, et al. Efficiency of curative and prophylactic treatment with rituximab in ADAMTS13-deficient thrombotic thrombocytopenic purpura: a study of 11 cases. *Blood* 2005;106(6):1932-7. doi: 10.1182/blood-2005-03-0848 [published Online First: 2005/06/04]

87. Kreuz W. von Willebrand's disease: from discovery to therapy - milestones in the last 25 years. *Haemophilia* 2008;14 Suppl 5:1-2. doi: 10.1111/j.1365-2516.2008.01846.x [published Online First: 2008/09/17]
88. De Meyer SF, Deckmyn H, Vanhoorelbeke K. von Willebrand factor to the rescue. *Blood* 2009;113(21):5049-57. doi: 10.1182/blood-2008-10-165621 [published Online First: 2009/03/26]
89. Sadler JE. A revised classification of von Willebrand disease. For the Subcommittee on von Willebrand Factor of the Scientific and Standardization Committee of the International Society on Thrombosis and Haemostasis. *Thromb Haemost* 1994;71(4):520-5. [published Online First: 1994/04/01]
90. Eikenboom J, Van Marion V, Putter H, et al. Linkage analysis in families diagnosed with type 1 von Willebrand disease in the European study, molecular and clinical markers for the diagnosis and management of type 1 VWD. *J Thromb Haemost* 2006;4(4):774-82. doi: 10.1111/j.1538-7836.2006.01823.x [published Online First: 2006/04/26]
91. James PD, Notley C, Hegadorn C, et al. The mutational spectrum of type 1 von Willebrand disease: Results from a Canadian cohort study. *Blood* 2007;109(1):145-54. doi: 10.1182/blood-2006-05-021105. [published Online First: 2006/12/28]
92. Lillicrap D. Von Willebrand disease - phenotype versus genotype: deficiency versus disease. *Thromb Res* 2007;120 Suppl 1:S11-6. doi: 10.1016/j.thromres.2007.03.014 [published Online First: 2007/05/11]
93. O'Brien LA, Sutherland JJ, Weaver DF, et al. Theoretical structural explanation for Group I and Group II, type 2A von Willebrand disease mutations. *J Thromb Haemost* 2005;3(4):796-7. doi: 10.1111/j.1538-7836.2005.01219.x [published Online First: 2005/04/22]
94. Federici AB, Mannucci PM, Castaman G, et al. Clinical and molecular predictors of thrombocytopenia and risk of bleeding in patients with von Willebrand disease type 2B: a cohort study of 67 patients. *Blood* 2009;113(3):526-34. doi: 10.1182/blood-2008-04-152280 [published Online First: 2008/09/23]
95. Goodeve AC. The genetic basis of von Willebrand disease. *Blood Rev* 2010;24(3):123-34. doi: 10.1016/j.blre.2010.03.003 [published Online First: 2010/04/23]
96. Connell NT, Flood VH, Brignardello-Petersen R, et al. ASH ISTH NHF WFH 2021 guidelines on the management of von Willebrand disease. *Blood Adv* 2021;5(1):301-25. doi: 10.1182/bloodadvances.2020003264 [published Online First: 2021/02/12]
97. Chen X, Cheng X, Zhang S, et al. ADAMTS13: An Emerging Target in Stroke Therapy. *Front Neurol* 2019;10:772. doi: 10.3389/fneur.2019.00772 [published Online First: 2019/08/06]
98. Favaloro EJ, Henry BM, Lippi G. Increased VWF and Decreased ADAMTS-13 in COVID-19: Creating a Milieu for (Micro)Thrombosis. *Semin Thromb Hemost* 2021;47(4):400-18. doi: 10.1055/s-0041-1727282 [published Online First: 2021/04/25]
99. Groeneveld DJ, Poole LG, Luyendyk JP. Targeting von Willebrand factor in liver diseases: A novel therapeutic strategy? *J Thromb Haemost* 2021;19(6):1390-408. doi: 10.1111/jth.15312 [published Online First: 2021/03/29]
100. Katneni UK, Ibla JC, Hunt R, et al. von Willebrand factor/ADAMTS-13 interactions at birth: implications for thrombosis in the neonatal period. *J Thromb Haemost* 2019;17(3):429-40. doi: 10.1111/jth.14374 [published Online First: 2018/12/30]

101. Yang J, Wu Z, Long Q, et al. Insights Into Immunothrombosis: The Interplay Among Neutrophil Extracellular Trap, von Willebrand Factor, and ADAMTS13. *Front Immunol* 2020;11:610696. doi: 10.3389/fimmu.2020.610696 [published Online First: 2020/12/22]
102. Ziliotto N, Bernardi F, Piazza F. Hemostasis components in cerebral amyloid angiopathy and Alzheimer's disease. *Neurol Sci* 2021;42(8):3177-88. doi: 10.1007/s10072-021-05327-7 [published Online First: 2021/05/28]
103. Arisz RA, de Vries JJ, Schols SEM, et al. Interaction of von Willebrand factor with blood cells in flow models: a systematic review. *Blood Adv* 2022;6(13):3979-90. doi: 10.1182/bloodadvances.2021006405 [published Online First: 2022/07/12]
104. Bratton DL, Henson PM. Neutrophil clearance: when the party is over, clean-up begins. *Trends Immunol* 2011;32(8):350-7. doi: 10.1016/j.it.2011.04.009 [published Online First: 2011/07/26]
105. Henson PM, Johnston RB, Jr. Tissue injury in inflammation. Oxidants, proteinases, and cationic proteins. *J Clin Invest* 1987;79(3):669-74. doi: 10.1172/JCI112869 [published Online First: 1987/03/01]
106. Weiss SJ. Tissue destruction by neutrophils. *N Engl J Med* 1989;320(6):365-76. doi: 10.1056/NEJM198902093200606 [published Online First: 1989/02/09]
107. Denorme F, Langhauser F, Desender L, et al. ADAMTS13-mediated thrombolysis of t-PA-resistant occlusions in ischemic stroke in mice. *Blood* 2016;127(19):2337-45. doi: 10.1182/blood-2015-08-662650 [published Online First: 2016/03/02]
108. South K, Denorme F, Salles C, II, et al. Enhanced activity of an ADAMTS-13 variant (R568K/F592Y/R660K/Y661F/Y665F) against platelet agglutination in vitro and in a murine model of acute ischemic stroke. *J Thromb Haemost* 2018;16(11):2289-99. doi: 10.1111/jth.14275 [published Online First: 2018/08/29]
109. De Meyer SF, Savchenko AS, Haas MS, et al. Protective anti-inflammatory effect of ADAMTS13 on myocardial ischemia/reperfusion injury in mice. *Blood* 2012;120(26):5217-23. doi: 10.1182/blood-2012-06-439935 [published Online First: 2012/08/24]
110. Zitomersky NL, Demers M, Martinod K, et al. ADAMTS13 Deficiency Worsens Colitis and Exogenous ADAMTS13 Administration Decreases Colitis Severity in Mice. *TH Open* 2017;1(1):e11-e23. doi: 10.1055/s-0037-1603927 [published Online First: 2018/01/30]
111. Wong SL, Goverman J, Staudinger C, et al. Recombinant human ADAMTS13 treatment and anti-NET strategies enhance skin allograft survival in mice. *Am J Transplant* 2020;20(4):1162-69. doi: 10.1111/ajt.15703 [published Online First: 2019/11/16]
112. Erpenbeck L, Demers M, Zsengeller ZK, et al. ADAMTS13 Endopeptidase Protects against Vascular Endothelial Growth Factor Inhibitor-Induced Thrombotic Microangiopathy. *J Am Soc Nephrol* 2016;27(1):120-31. doi: 10.1681/ASN.2014121165 [published Online First: 2015/06/04]
113. Johnston I, Sarkar A, Hayes V, et al. Recognition of PF4-VWF complexes by heparin-induced thrombocytopenia antibodies contributes to thrombus propagation. *Blood* 2020;135(15):1270-80. doi: 10.1182/blood.2018881607 [published Online First: 2020/02/23]
114. Zhou S, Guo J, Zhao L, et al. ADAMTS13 inhibits oxidative stress and ameliorates progressive chronic kidney disease following ischaemia/reperfusion injury. *Acta Physiol (Oxf)* 2021;231(3):e13586. doi: 10.1111/apha.13586 [published Online First: 2020/11/24]
115. Kleinveld DJB, Simons DDG, Dekimpe C, et al. Plasma and rhADAMTS13 reduce trauma-induced organ failure by restoring the ADAMTS13-VWF axis. *Blood Adv*

2021;5(17):3478-91. doi: 10.1182/bloodadvances.2021004404 [published Online First: 2021/09/11]
116. Yamamoto K, Murphy G, Troeberg L. Extracellular regulation of metalloproteinases. *Matrix Biol* 2015;44-46:255-63. doi: 10.1016/j.matbio.2015.02.007 [published Online First: 2015/02/24]
117. Guo C, Tsigkou A, Lee MH. ADAMTS13 and 15 are not regulated by the full length and N-terminal domain forms of TIMP-1, -2, -3 and -4. *Biomed Rep* 2016;4(1):73-78. doi: 10.3892/br.2015.535 [published Online First: 2016/02/13]
118. Shelat SG, Ai J, Zheng XL. Molecular biology of ADAMTS13 and diagnostic utility of ADAMTS13 proteolytic activity and inhibitor assays. *Semin Thromb Hemost* 2005;31(6):659-72. doi: 10.1055/s-2005-925472 [published Online First: 2006/01/03]
119. Singh K, Madarati H, Sohrabipour S, et al. Metalloprotease domain latency protects ADAMTS13 against broad- spectrum inhibitors of metalloproteases while maintaining activity towards VWF. *J Thromb Haemost* 2023 doi: 10.1016/j.jtha.2023.03.021 [published Online First: 2023/03/30]
120. Rose KWJ, Taye N, Karoulias SZ, et al. Regulation of ADAMTS Proteases. *Front Mol Biosci* 2021;8:701959. doi: 10.3389/fmolb.2021.701959 [published Online First: 2021/07/17]
121. Somerville RP, Longpre JM, Apel ED, et al. ADAMTS7B, the full-length product of the ADAMTS7 gene, is a chondroitin sulfate proteoglycan containing a mucin domain. *J Biol Chem* 2004;279(34):35159-75. doi: 10.1074/jbc.M402380200 [published Online First: 2004/06/12]
122. Zheng X, Chung D, Takayama TK, et al. Structure of von Willebrand factor-cleaving protease (ADAMTS13), a metalloprotease involved in thrombotic thrombocytopenic purpura. *J Biol Chem* 2001;276(44):41059-63. doi: 10.1074/jbc.C100515200 [published Online First: 2001/09/15]
123. Furlan M, Robles R, Morselli B, et al. Recovery and half-life of von Willebrand factor-cleaving protease after plasma therapy in patients with thrombotic thrombocytopenic purpura. *Thromb Haemost* 1999;81(1):8-13. [published Online First: 1999/05/29]
124. Robertson J, Lillicrap D, James PD. Von Willebrand disease. *Pediatr Clin North Am* 2008;55(2):377-92, viii-ix. doi: 10.1016/j.pcl.2008.01.008 [published Online First: 2008/04/03]
125. Ono T, Mimuro J, Madoiwa S, et al. Severe secondary deficiency of von Willebrand factor-cleaving protease (ADAMTS13) in patients with sepsis-induced disseminated intravascular coagulation: its correlation with development of renal failure. *Blood* 2006;107(2):528-34. doi: 10.1182/blood-2005-03-1087 [published Online First: 2005/09/29]
126. Feys HB, Vandeputte N, Palla R, et al. Inactivation of ADAMTS13 by plasmin as a potential cause of thrombotic thrombocytopenic purpura. *J Thromb Haemost* 2010;8(9):2053-62. doi: 10.1111/j.1538-7836.2010.03942.x [published Online First: 2010/06/18]
127. Galbusera M, Ruggenenti P, Noris M, et al. alpha 1-Antitrypsin therapy in a case of thrombotic thrombocytopenic purpura. *Lancet* 1995;345(8944):224-5. doi: 10.1016/s0140-6736(95)90224-4 [published Online First: 1995/01/28]
128. Crawley JT, Lam JK, Rance JB, et al. Proteolytic inactivation of ADAMTS13 by thrombin and plasmin. *Blood* 2005;105(3):1085-93. doi: 10.1182/blood-2004-03-1101 [published Online First: 2004/09/25]

129. Garland KS, Reitsma SE, Shirai T, et al. Removal of the C-Terminal Domains of ADAMTS13 by Activated Coagulation Factor XI induces Platelet Adhesion on Endothelial Cells under Flow Conditions. *Front Med (Lausanne)* 2017;4:232. doi: 10.3389/fmed.2017.00232 [published Online First: 2018/01/13]
130. Hiura H, Matsui T, Matsumoto M, et al. Proteolytic fragmentation and sugar chains of plasma ADAMTS13 purified by a conformation-dependent monoclonal antibody. *J Biochem* 2010;148(4):403-11. doi: 10.1093/jb/mvq075 [published Online First: 2010/07/14]
131. Tersteeg C, de Maat S, De Meyer SF, et al. Plasmin cleavage of von Willebrand factor as an emergency bypass for ADAMTS13 deficiency in thrombotic microangiopathy. *Circulation* 2014;129(12):1320-31. doi: 10.1161/CIRCULATIONAHA.113.006727 [published Online First: 2014/01/23]
132. Lam JK, Chion CK, Zanardelli S, et al. Further characterization of ADAMTS-13 inactivation by thrombin. *J Thromb Haemost* 2007;5(5):1010-8. doi: 10.1111/j.1538-7836.2007.02514.x [published Online First: 2007/03/16]
133. Shin Y, Miyake H, Togashi K, et al. Proteolytic inactivation of ADAMTS13 by plasmin in human plasma: risk of thrombotic thrombocytopenic purpura. *J Biochem* 2018;163(5):381-89. doi: 10.1093/jb/mvx084 [published Online First: 2017/12/12]
134. Kokame K, Nobe Y, Kokubo Y, et al. FRETS-VWF73, a first fluorogenic substrate for ADAMTS13 assay. *Br J Haematol* 2005;129(1):93-100. doi: 10.1111/j.1365-2141.2005.05420.x [published Online First: 2005/04/02]
135. Rothschild MA, Oratz M, Schreiber SS. Serum albumin. *Hepatology* 1988;8(2):385-401. doi: 10.1002/hep.1840080234 [published Online First: 1988/03/01]
136. Luddington R, Baglin T. Clinical measurement of thrombin generation by calibrated automated thrombography requires contact factor inhibition. *J Thromb Haemost* 2004;2(11):1954-9. doi: 10.1111/j.1538-7836.2004.00964.x [published Online First: 2004/11/20]
137. Michels A, Swystun LL, Mewburn J, et al. Investigating von Willebrand Factor Pathophysiology Using a Flow Chamber Model of von Willebrand Factor-platelet String Formation. *J Vis Exp* 2017(126) doi: 10.3791/55917 [published Online First: 2017/08/23]
138. Chen X, Zaro JL, Shen WC. Fusion protein linkers: property, design and functionality. *Adv Drug Deliv Rev* 2013;65(10):1357-69. doi: 10.1016/j.addr.2012.09.039 [published Online First: 2012/10/03]
139. Yu S, Liu W, Fang J, et al. AFM Imaging Reveals Multiple Conformational States of ADAMTS13. *J Biol Eng* 2019;13:9. doi: 10.1186/s13036-018-0102-y [published Online First: 2019/01/27]
140. Roose E, Schelpe AS, Joly BS, et al. An open conformation of ADAMTS-13 is a hallmark of acute acquired thrombotic thrombocytopenic purpura. *J Thromb Haemost* 2018;16(2):378-88. doi: 10.1111/jth.13922 [published Online First: 2017/12/10]
141. Cao E, Chen Y, Cui Z, et al. Effect of freezing and thawing rates on denaturation of proteins in aqueous solutions. *Biotechnol Bioeng* 2003;82(6):684-90. doi: 10.1002/bit.10612 [published Online First: 2003/04/04]
142. Jankowska KI, Katneni U, Lin BC, et al. An Optimized Purification Design for Extracting Active ADAMTS13 from Conditioned Media. *Processes* 2022; 10(2).
143. Kangro K, Roose E, Dekimpe C, et al. Improvement of recombinant ADAMTS13 production through a more optimal signal peptide or an N-terminal fusion protein. *J Thromb*

Haemost 2022;20(10):2379-85. doi: 10.1111/jth.15819 [published Online First: 2022/07/17]
144. Doi M, Matsui H, Takeda H, et al. ADAMTS13 safeguards the myocardium in a mouse model of acute myocardial infarction. *Thromb Haemost* 2012;108(6):1236-8. doi: 10.1160/TH12-09-0674 [published Online First: 2012/10/12]
145. Tersteeg C, Schiviz A, De Meyer SF, et al. Potential for Recombinant ADAMTS13 as an Effective Therapy for Acquired Thrombotic Thrombocytopenic Purpura. *Arterioscler Thromb Vasc Biol* 2015;35(11):2336-42. doi: 10.1161/ATVBAHA.115.306014 [published Online First: 2015/09/05]
146. Zhao BQ, Chauhan AK, Canault M, et al. von Willebrand factor-cleaving protease ADAMTS13 reduces ischemic brain injury in experimental stroke. *Blood* 2009;114(15):3329-34. doi: 10.1182/blood-2009-03-213264 [published Online First: 2009/08/19]
147. Fitzmaurice DA, Blann AD, Lip GY. Bleeding risks of antithrombotic therapy. *BMJ* 2002;325(7368):828-31. doi: 10.1136/bmj.325.7368.828 [published Online First: 2002/10/12]
148. Walker AM, Jick H. Predictors of bleeding during heparin therapy. *JAMA* 1980;244(11):1209-12. [published Online First: 1980/09/12]
149. Wang L, Fan W, Cai P, et al. Recombinant ADAMTS13 reduces tissue plasminogen activator-induced hemorrhage after stroke in mice. *Ann Neurol* 2013;73(2):189-98. doi: 10.1002/ana.23762 [published Online First: 2013/01/03]
150. Kopic A, Benamara K, Piskernik C, et al. Preclinical assessment of a new recombinant ADAMTS-13 drug product (BAX930) for the treatment of thrombotic thrombocytopenic purpura. *J Thromb Haemost* 2016;14(7):1410-9. doi: 10.1111/jth.13341 [published Online First: 2016/07/03]
151. Chapman SN, Mehndiratta P, Johansen MC, et al. Current perspectives on the use of intravenous recombinant tissue plasminogen activator (tPA) for treatment of acute ischemic stroke. *Vasc Health Risk Manag* 2014;10:75-87. doi: 10.2147/VHRM.S39213 [published Online First: 2014/03/05]
152. Fan M, Xu H, Wang L, et al. Tissue Plasminogen Activator Neurotoxicity is Neutralized by Recombinant ADAMTS 13. *Sci Rep* 2016;6:25971. doi: 10.1038/srep25971 [published Online First: 2016/05/18]
153. Nakano T, Irie K, Hayakawa K, et al. Delayed treatment with ADAMTS13 ameliorates cerebral ischemic injury without hemorrhagic complication. *Brain Res* 2015;1624:330-35. doi: 10.1016/j.brainres.2015.07.027 [published Online First: 2015/08/10]
154. Cai W, Liu S, Hu M, et al. Functional Dynamics of Neutrophils After Ischemic Stroke. *Transl Stroke Res* 2020;11(1):108-21. doi: 10.1007/s12975-019-00694-y [published Online First: 2019/03/09]
155. Urisono Y, Sakata A, Matsui H, et al. Von Willebrand Factor Aggravates Hepatic Ischemia-Reperfusion Injury by Promoting Neutrophil Recruitment in Mice. *Thromb Haemost* 2018;118(4):700-08. doi: 10.1055/s-0038-1636529 [published Online First: 2018/04/05]
156. Mesters RM, Mannucci PM, Coppola R, et al. Factor VIIa and antithrombin III activity during severe sepsis and septic shock in neutropenic patients. *Blood* 1996;88(3):881-6. [published Online First: 1996/08/01]
157. Esmon CT. Role of coagulation inhibitors in inflammation. *Thromb Haemost* 2001;86(1):51-6. [published Online First: 2001/08/07]

158. Levi M. The imbalance between tissue factor and tissue factor pathway inhibitor in sepsis. *Crit Care Med* 2002;30(8):1914-5. doi: 10.1097/00003246-200208000-00046 [published Online First: 2002/08/07]
159. Madoiwa S, Nunomiya S, Ono T, et al. Plasminogen activator inhibitor 1 promotes a poor prognosis in sepsis-induced disseminated intravascular coagulation. *Int J Hematol* 2006;84(5):398-405. doi: 10.1532/IJH97.05190 [published Online First: 2006/12/26]
160. Singh K, Kwong AC, Madarati H, et al. Characterization of ADAMTS13 and von Willebrand factor levels in septic and non-septic ICU patients. *PLoS One* 2021;16(2):e0247017. doi: 10.1371/journal.pone.0247017 [published Online First: 2021/02/20]
161. Peetermans M, Meyers S, Liesenborghs L, et al. Von Willebrand factor and ADAMTS13 impact on the outcome of Staphylococcus aureus sepsis. *J Thromb Haemost* 2020;18(3):722-31. doi: 10.1111/jth.14686 [published Online First: 2019/11/24]
162. Nguyen TC, Liu A, Liu L, et al. Acquired ADAMTS-13 deficiency in pediatric patients with severe sepsis. *Haematologica* 2007;92(1):121-4. doi: 10.3324/haematol.10262 [published Online First: 2007/01/19]
163. Lerolle N, Dunois-Larde C, Badirou I, et al. von Willebrand factor is a major determinant of ADAMTS-13 decrease during mouse sepsis induced by cecum ligation and puncture. *J Thromb Haemost* 2009;7(5):843-50. doi: 10.1111/j.1538-7836.2009.03313.x [published Online First: 2009/02/04]
164. Corken A, Russell S, Dent J, et al. Platelet glycoprotein Ib-IX as a regulator of systemic inflammation. *Arterioscler Thromb Vasc Biol* 2014;34(5):996-1001. doi: 10.1161/ATVBAHA.113.303113 [published Online First: 2014/02/08]

APPENDIX 1: MUTATIONS

Single-letter amino acid sequence of wild-type ADAMTS13:

MAAGGILHLELLVAVGPDVFQAHQEDTERYVLTNLNIGAELLRDPSLGAQFRVH
LVKMVILTEPEGAPNITANLTSSLLSVCGWSQTINPEDDTDPGHADLVLYITRFDL
ELPDGNRQVRGVTQLGGACSPTWSCLITEDTGFDLGVTIAHEIGHSFGLEHDGAP
GSGCGPSGHVMASDGAAPRAGLAWSPCSRRQLLSLLSAGRARCVWDPPRPQPGS
AGHPPDAQPGLYYSANEQCRVAFGPKAVACTFAREHLDMCQALSCHTDPLDQS
SCSRLLVPLLDGTECGVEKWCSKGRCRSLVELTPIAAVHGRWSSWGPRSPCSRSC
GGGVVTRRRQCNNPRPAFGGRACVGADLQAEMCNTQACEKTQLEFMSQQCAR
TDGQPLRSSPGGASFYHWGAAVPHSQGDALCRHMCRAIGESFIMKRGDSFLDGT
RCMPSGPREDGTLSLCVSGSCRTFGCDGRMDSQQVWDRCQVCGGDNSTCSPRK
GSFTAGRAREYVTFLTVTPNLTSVYIANHRPLFTHLAVRIGGRYVVAGKMSISPN
TTYPSLLEDGRVEYRVALTEDRLPRLEEIRIWGPLQEDADIQVYRRYGEEYGNLT
RPDITFTYFQPKPRQAWVWAAVRGPCSVSCGAGLRWVNYSCLDQARKELVETV
QCQGSQQPPAWPEACVLEPCPPYWAVGDFGPCSASCGGGLRERPVRCVEAQGSL
LKTLPPARCRAGAQQPAVALETCNPQPCPARWEVSEPSSCTSAGGAGLALENET
CVPGADGLEAPVTEGPGSVDEKLPAPEPCVGMSCPPGWGHLDATSAGEKAPSPW
GSIRTGAQAAHVWTPAAGSCSVSCGRGLMELRFLCMDSALRVPVQEELCGLASK
PGSRREVCQAVPCPARWQYKLAACSVSCGRGVVRRILYCARAHGEDDGEEILLD
TQCQGLPRPEPQEACSLEPCPPRWKVMSLGPCSASCGLGTARRSVACVQLDQGQ
DVEVDEAACAALVRPEASVPCLIADCTYRWHVGTWMECSVSCGDGIQRRRDTC
LGPQAQAPVPADFCQHLPKPVTVRGCWAGPCVGQGTPSLVPHEEAAAPGRTTAT
PAGASLEWSQARGLLFSPAPQPRRLLPGPQENSVQSSACGRQHLEPTGTIDMRGP
GQADCAVAIGRPLGEVVTLRVLESSLNCSAGDMLLLWGRLTWRKMCRKLLDMT
FSSKTNTLVVRQRCGRPGGGVLLRYGSQLAPETFYRECDMQLFGPWGEIVSPSLS
PATSNAGGCRLFINVAPHARIAIHALATNMGAGTEGANASYILIRDTHSLRTTAFH
GQQVLYWESESSQAEMEFSEGFLKAQASLRGQYWTLQSWVPEMQDPQSWKGK
EGT

I380G (orange), T4L (red), T8L (green) mutations:

MAAGGILHLELLVAVGPDVFQAHQEDTERYVLTNLNIGAELLRDPSLGAQFRVH
LVKMVILTEPEGAPNITANLTSSLLSVCGWSQTINPEDDTDPGHADLVLYITRFDL
ELPDGNRQVRGVTQLGGACSPTWSCLITEDTGFDLGVTIAHEIGHSFGLEHDGAP
GSGCGPSGHVMASDGAAPRAGLAWSPCSRRQLLSLLSAGRARCVWDPPRPQPGS

AGHPPDAQPGLYYSANEQCRVAFGPKAVACTFAREHLDMCQALSCHTDPLDQS
SCSRLLVPLLDGTECGVEKWCSKGRCRSLVELTPIAAVHGRWSSWGPRSPCSRSC
GGGVVTRRRQCNNPRPAFGGRACVGADLQAEMCNTQACEKTQLEFMSQQCAR
TDGQPLRSSPGGASFYHWGAAVPHSQGDALCRHMCRAIGESFIMKRGDSFLDGT
RCMPSGPREDGTLSLCVSGSCRTFGCDGRMDSQQVWDRCQVCGGDNSTCSPRK
GSFTAGRAREYVTFLTVTPNLTSVYIANHRPLFTHLAVRIGGRYVVAGKMSISPN
TTYPSLLEDGRVEYRVALTEDRLPRLEEIRIWGPLQEDADIQVYRRYGEEYGNLT
RPDITFTYFQPKPRQAWVWAAVRGPCSVSCGAGLRWVNYSCLDQARKELVETV
QCQGSQQPPAWPEACVLEPCPPYWAVGDFGPCSASCGGGLRERPVRCVEAQGSL
LKTLPPARCRAGAQQPAVALETCNPQPCPARWEVSEPSSCTSAGGAGLALENET
CVPGADGLEAPVTEGPGSVDEKLPAPEPCVGMSCPPGGGSGGGSGGGSGGGSGG
GSGGGSGGGSHVWTPAAGSCSVSCGRGLMELRFLCMDSALRVPVQEELCGLAS
KPGSRREVCQAVPCPARWQYKLAACSVSCGRGVVRRILYCARAHGEDDGEEILL
DTQCQGLPRPEPQEACSLEPCPPRWKVMSLGPCSASCGLGTARRSVACVQLDQG
QDVEVDEAACAALVRPEASVPCLIADCTYRWHVGTWMECSVSCGDGIQRRRDT
CLGPQAQAPVPADFCQHLPKPVTVRGCWAGPCVGQGGGSGGGSGGGSGGGSGG
GSGGGSGGGSGGGSGGGSGGGSGGGSGGGSGGGSGGGSGSCGRQHLEPTGTID
MRGPGQADCAVAIGRPLGEVVTLRVLESSLNCSAGDMLLLWGRLTWRKMCRKL
LDMTFSSKTNTLVVRQRCGRPGGGVLLRYGSQLAPETFYRECDMQLFGPWGEIV
SPSLSPATSNAGGCRLFINVAPHARIAIHALATNMGAGTEGANASYILIRDTHSLR
TTAFHGQQVLYWESESSQAEMEFSEGFLKAQASLRGQYWTLQSWVPEMQDPQS
WKGKEGT

APPENDIX 2: FLOW SYSTEM SCHEMATIC

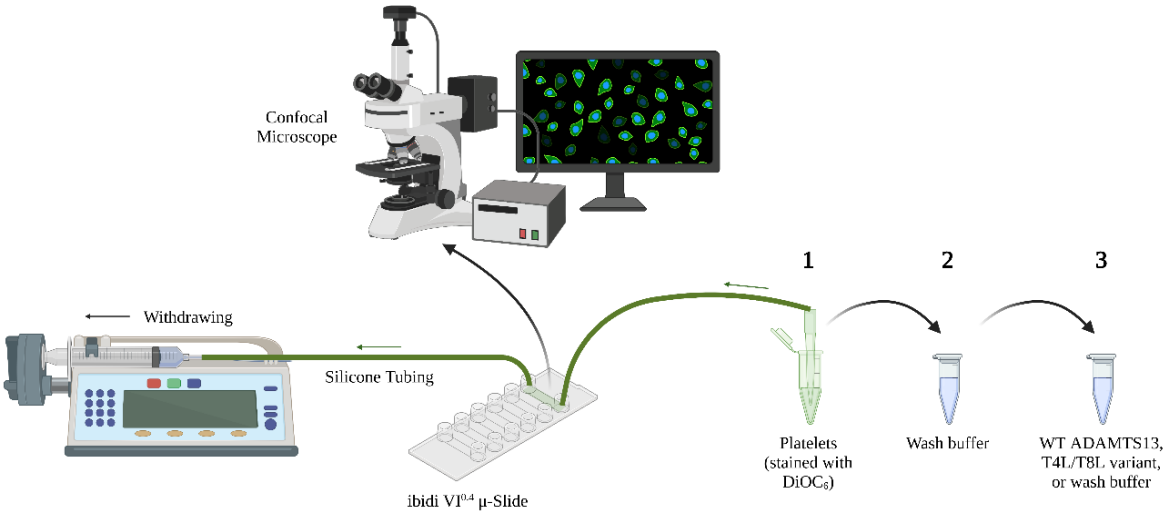

Figure 1. Schematic of the flow system assembled for the VWF-platelet string cleavage assay.

APPENDIX 3: CONTROL MEASURES

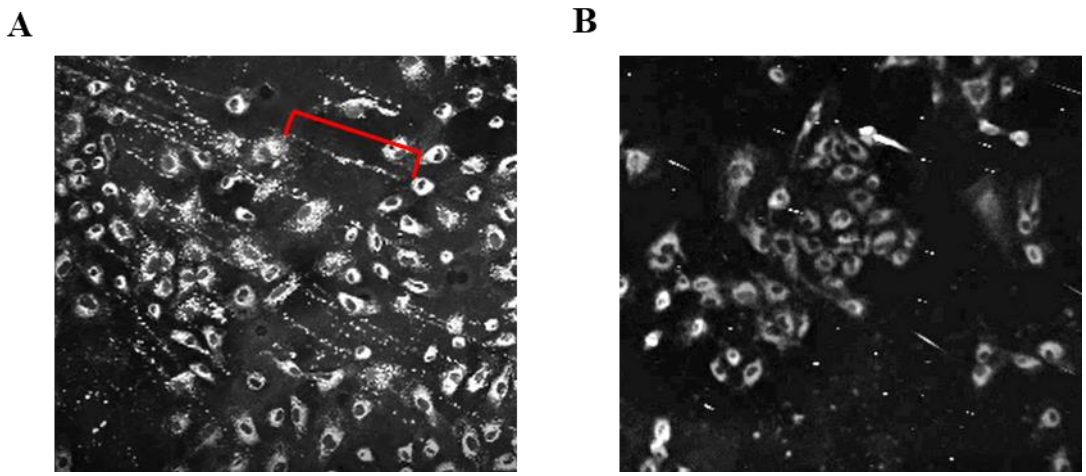

Figure 1. Validating the presence of VWF in the VWF-platelet string cleavage assay. Channels lined with HUVECs were first perfused with 2 mL of ADAMTS13 reaction buffer to shear-activate the cells, followed immediately by (A) 2 mL of 1:100 polyclonal anti-VWF antibody to phosphate-buffered saline (PBS), or (B) 2 mL of PBS alone. 3 mL of DiOC6-stained platelet solution (approximately 200 000 cells/µL) was then perfused over each channel. Representative images of the channels nearing the end of platelet perfusion are presented. An example of a VWF-platelet string is outlined end-to-end by the red square bracket (A).